Strål
säkerhets
myndigheten
Swedish Radiation Safety Authority

Author: Tobias Bolinder
Iradj Sattari-Far

Research

2011:19

Experimental evaluation of influence from residual stresses on crack initiation and ductile crack growth at high primary loads

Report number: 2011:19 ISSN: 2000-0456
Available at www.stralsakerhetsmyndigheten.se

SSM perspective

Background

Cracked components are usually subjected to loads causing both primary and secondary stresses, e.g. welding components. Engineering assessment approaches, such as the ASME XI code and the R6 procedure, are commonly used to conduct integrity assessment of such components. There has been an ongoing debate how to treat secondary stresses using engineering assessment methods. The nature of these assessment approaches is to give reasonably conservative assessments. These two approaches treat the issue of secondary stresses differently. The ASME XI code does not consider weld-induced residual stresses in some materials, for instance stainless steel welds. The R6-method on the other hand tends to give overly conservative assessment results.

The significance of the secondary stresses for cracks in ductile materials within nuclear applications has been studied earlier using an analytical approach by a SSM-financed study (SSM Research Report 2009:27). In that study a deterministic safety evaluation procedure was proposed in which the residual stresses were weighted down for sufficiently ductile materials. In the current study this safety evaluation procedure is investigated by performing experiments.

Objectives

The objective of the study is to investigate the significance of residual stresses for ductile fracture and to experimentally verify a proposed deterministic safety evaluation procedure for treatment of certain secondary stresses for ductile materials.

Results

Based on the experimental and numerical investigation on the effects of residual stresses in cracked specimens of ductile materials the following conclusions may be made:

- The experimental results clearly show a decreasing influence from the residual stresses on the *J*-integral for increasing primary load. A clear trend could be seen for both material that the influence from the residual stresses start to disappear entirely for the plastic collapse parameter L_r >1. For the material A533B the influence from the residual stresses on J was seen to disappear entirely for L_r >1.
- The experimental results clearly show a decreasing influence from the residual stresses on the *J*-integral for increasing primary load. Crack initiation in the experiments was achieved at L_r values between 0.9-1.1. Only small effects from the residual stress field were seen on crack initiation for the specimens which had crack initiation at L_r values between 0.9 and 1.0, and no effects from the residual stress field on crack initiation were seen for the specimens loaded at L_r values between 1.0 and 1.1.
- It was shown that the residual stress field had no measurable influence on the stable crack growth of the specimens at L_r > 1.

- The presented results strengthen the validity of a suggested deterministic safety evaluation procedure where it is proposed to start the weighting down of the secondary safety factor $SF_K^{secondary}$ at a predicted value at fracture of L_r =0.8. The suggested evaluation procedure is valid for sufficiently ductile materials such as austenitic stainless steels, nickel based alloys and ferritic steels in the upper shelf regime.

Need for further research

The results can be used in safety assessments of cracked components of ductile materials. More research is needed in order to find a more general engineering procedure for the treatment of cracked components subjected to different secondary stresses in different materials.

Project information

Contact person SSM: Björn Brickstad
Reference: SSM 2008/321

Strål
säkerhets
myndigheten
Swedish Radiation Safety Authority

Author: Tobias Bolinder and Iradj Sattari-Far
Inspecta Nuclear AB, Sweden

2011:19

Experimental evaluation of influence from residual stresses on crack initiation and ductile crack growth at high primary loads

Date: June 2011
Report number: 2011:19 **ISSN:** 2000-0456
Available at www.stralsakerhetsmyndigheten.se

Table of content ***Page***

ACKNOWLEDGEMENT

The authors are grateful for the financial support of the Swedish Radiation Safety Authority (SSM) and the nuclear power plant owners (Kraftbolagen). This project was conducted in close collaboration with the department of Solid Mechanics at KTH, where the theoretical expertise received from Jonas Faleskog during the project and the experimental expertise from Hans Öberg are very much appreciated. The authors would also like to thank SSAB Oxelösund and SERCO UK for assisting in supplying the materials used in the experiments.

1 INTRODUCTION

Engineering components, like components in nuclear power plants, can be subjected to loads that cause primary or secondary stresses (for instance welding residual stresses). Engineering assessment approaches, like the ASME XI code and the R6 procedure, are commonly used to conduct integrity assessment of such components. The nature of these assessment approaches is to give reasonably conservative assessments. These two approaches treat the issue of secondary stresses differently. The ASME XI code does not consider weld-induced residual stresses in some materials, for instance stainless steel welds, and the R6-method may give overly conservative assessment results. The treatment of secondary stresses in the R6-based ProSACC handbook, Dillström et al [1], is believed to be too conservative for ductile materials.

There are experimental evidences that the contribution of residual stresses to fracture diminishes as the degree of yielding increases. Results on a series of experiments by Sharples et al [2-4] and Mirzaee-Sisan et al [5-6] showed that at low load levels, i.e. small L_r, the influence of the residual stresses was large, but at high load levels, around $L_r = 1$, welding residual stresses were of little importance. A literature study on this matter was conducted by Sattari-Far [7], giving the following remarks on the effects of secondary stresses on the crack driving forces in cracked bodies:

- For high levels of primary loads ($L_r \geq 1.0$), the significance of secondary stresses are negligible in ductile materials.
- For loads that are mostly secondary (e.g. thermal shocks) and for materials which are not ductile enough, the effects of secondary stresses can be significant.

The significance of the secondary stresses for defects (cracks) in ductile materials within nuclear applications was studied by Dillström et al [8]. Both thin-walled and thick-walled pipes containing surface cracks were studied. This was done by calculating the relative contribution from the weld residual stresses to *J* and CTOD. Based on the outcome of this study, an analysis strategy for fracture assessment of defects in ductile materials of nuclear components has been proposed to more realistically handle the contribution of secondary stresses to the fracture parameters *J* or CTOD. In this new deterministic safety evaluation system, new safety factors are defined that differentiate between primary stresses and secondary stresses. The new safety factors against fracture described by K_I differentiate between $SF_K^{primary}$ (relating to primary stresses) and $SF_K^{secondary}$ (relating to secondary stresses). According to this procedure, the safety factor related to secondary stresses decreases based on the predicted value of *Lr* at fracture. The idea is shown in Figure 1.1. As can be seen from Figure 1.1, the contribution from secondary stresses becomes negligible for high L_r -values.

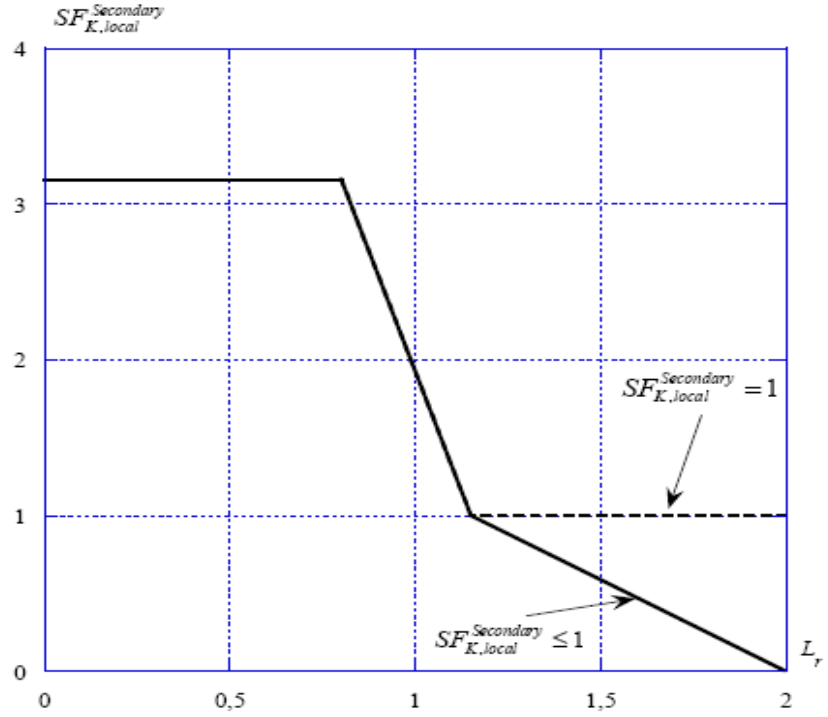

Figure 1.1: Safety factor related to secondary stresses proposed by Dillström et al [8] to be used in the R6-based ProSACC handbook.

In order to validate the new procedure, proposed by Dillström et al [8], for assessment of cracks in ductile materials with presence of secondary stresses, more experimental results was needed. Sattari-Far [7] investigated the possibilities to conduct suitable experiments in Sweden for this purpose.

The purpose of this study is therefore to verify the proposed strategy for fracture assessment of defects in ductile materials, as presented in Figure 1.1. Single-notched specimens containing surface edge cracks are used for this purpose. The specimens were pre-loaded in compression to introduce the residual stress field. The test program covered two material types; Weldox 700 (high strength low alloyed steels) and A533 reactor pressure vessel steel. The overall target of the tests was to obtain ductile crack initiation at a load level close to L_r = 1.0. The need for these kinds of experiments was expressed in [8]. Three test programs were conducted to cover the affecting parameters in obtaining the objectives of the study.

2 CHOICE OF PRE-LOADING AND SPECIMEN GEOMETRY

The purpose of the experimental programs where to examine the influence of residual stresses on crack initiation for high primary loads. For this to be successful a proper test specimen should be decided on. The method of introducing the residual stresses was chosen to be as simplistic as possible, to not introduce uncertainties or factors that could be hard to predict and model, and also be able to isolate the actual influence of the residual stresses. Thus, a test specimen resembling a standard 3PB test specimen was chosen. A pre-study was conducted on different influencing factors on the residual stress field and the needed geometry and size of the test specimens. The chosen method for introducing the residual stress field was using in-plane compression. This method has been successfully used earlier by Mirzaee-Sisan et al [5]. The actual fracture tests were then performed similarly to a standard *J-R* testing for specimens with and without residual stresses. The geometries of the test specimens in the different test programs were chosen to obtain crack initiation for different levels of primary loads. This is discussed below in chapter 2.2. Different materials where also studied in the test programs. The reason for this was to be able to get initiation around $L_r = 1$ ($L_r = P/P_L$). For this to be possible, materials with high enough hardening were needed.

2.1 Introduction of residual stresses

The chosen method of introducing the residual stresses was by in-plane compression of a notched test specimen as shown in Figure 2.1.

Figure 2.1: In-plane compression of notched test specimen.

The in-plane compression of the specimen leads to a stress concentration at the notch with compressive stresses normal to the crack surface during the loading. The in-plane compression needs to be large enough to get plastic deformations. When the specimen is unloaded a residual stress field is introduced due to the fact that the material was deformed plastically. Since the stresses normal to the crack surface are compressive near the notch during the loading a tensile residual stress field would be introduced at the notch see Figure 2.2.

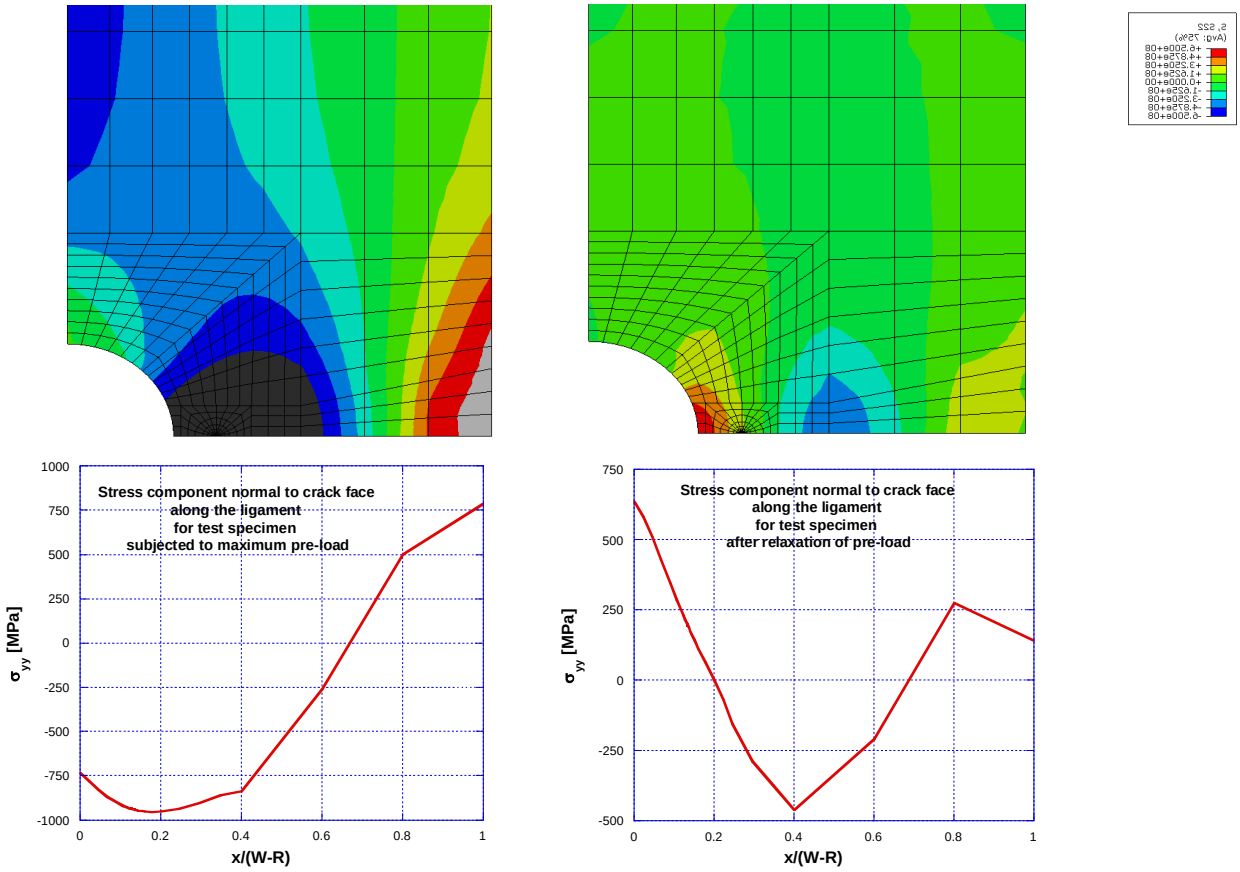

Figure 2.2: Stresses normal to crack surface during pre-loading and after pre-loading.

To obtain a zone with tensile residual stresses in front of the crack tip as large as possible, different factors influencing the residual stress field were studied by FE-analyses. All the FE-analyses carried out throughout this project used the FEM code ABAQUS [9]. The influencing factors examined are as listed below.

1. The size and shape of the notch
2. Type of pre-loading
3. Placement of pre-load
4. Magnitude of pre-load
5. Introducing the fatigue crack before or after pre-loading
6. Crack depth
7. Material yield strength
8. Material hardening

Several FE-models were created and analysed to get an optimal design of the test specimen to give a large as possible tensile residual stress field without introducing any new difficulties. For some factors, different undesired effects were working against a large tensile residual stress field. One example of such a factor is the crack depth. A shallow crack would give a larger residual stress field in front of the crack tip, but it would also introduce constraint effects. A shallower crack than the one chosen for this study would introduce some difficulties during the actual *J*-R testing. In this case both factors needed to be considered and weighted against each other. Below some of the relevant analyses are briefly described.

2.1.1 Effects from size and shape of the notch

Different shapes and sizes of the notch were examined to study these effects on the size of the tensile residual stress field. In Figure 2.3 two of the examined notch shapes a simple circular and a more complicated shape are shown.

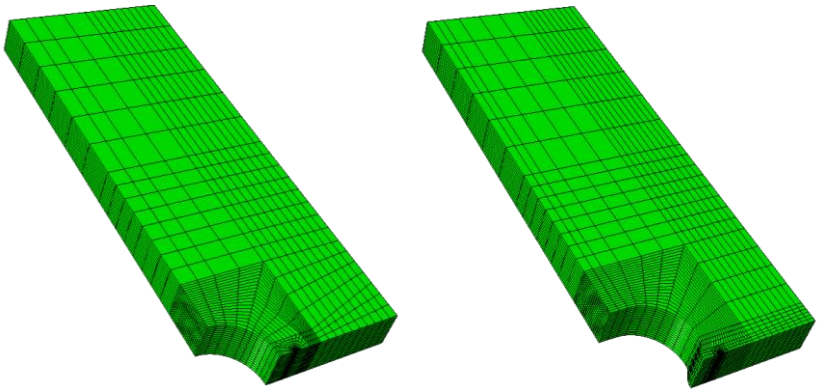

Simple circular notch Weilin notch

Figure 2.3: Different examined notch shapes.

It could be seen that after the crack was introduced, the effect of the shape of the notch was not as significant as it was before the crack was introduced, see Figure 2.4. From this it was decided that a simple circular notch would be used.

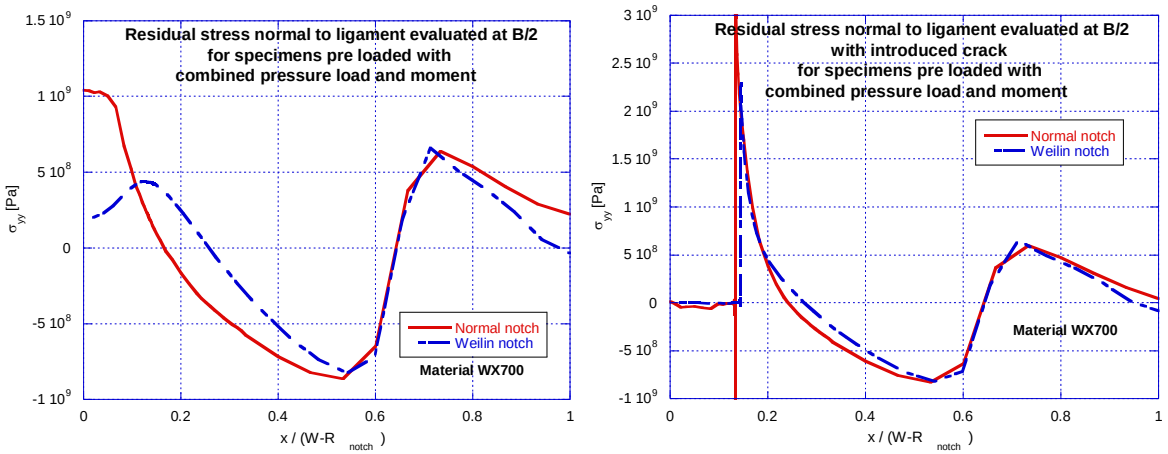

Figure 2.4: Residual stress normal to the crack surface before and after introduction of the crack for two different shaped notches.

The size of the notch had minor influence on the size of the tensile residual stress field see Figure 2.5. Further analyses gave an optimum size. From the analyses of a half circular notch with a radius depending on the width of the specimen was chosen. The relationship between the width of the specimen and the radius of the notch was chosen as $R=0.25W$.

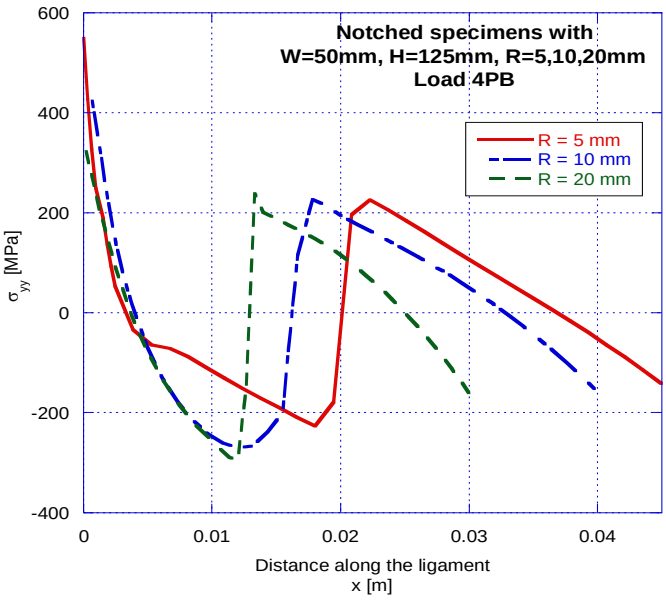

Figure 2.5: Influence on the residual stress field from the size of the notch.

2.1.2 Type and placement of pre-loading

Two types of loading were examined; a pure moment load created by four-point-bending (4PB) and a combined compression and bending load. As can be seen in Figure 2.6, the combined compression and bending load was the better choice.

Furthermore the placement along the specimen of the combined compression and bending load was also examined to receive a maximum size of the tensile residual stress field in front of the crack tip. This placement was related to the radius of the notch since this gave the distribution between pure compression and pure bending. From these analyses a relationship between the radius and the placement l_1 was chosen as l_1=0.8R.

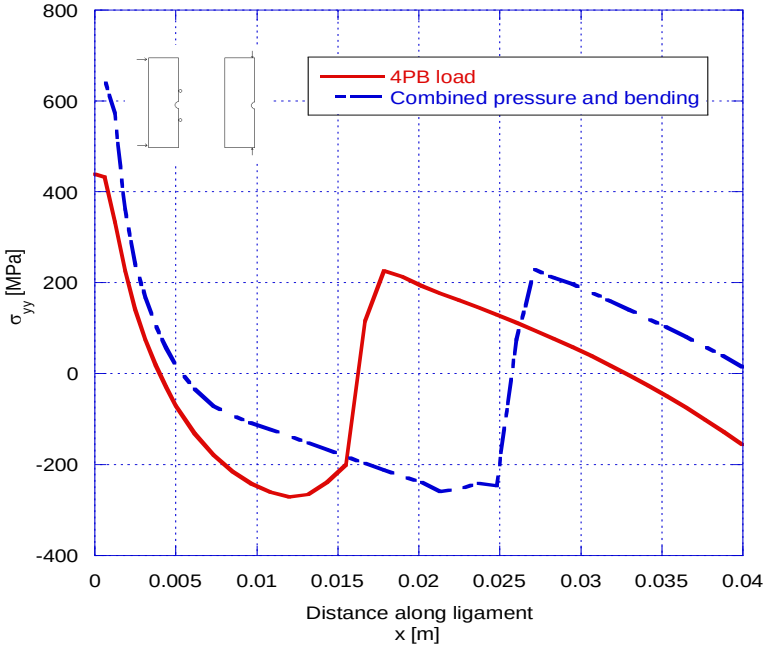

Figure 2.6: Influence on the residual stress field from the type of loading used during pre-loading.

2.1.3 Magnitude of pre-load

The magnitude of the pre-load was shown to not influence the size of the residual stress field in a significant way. It did however influence the magnitude of the tensile residual stress in front of the crack tip as can be seen in Figure 2.7. The magnitude of the pre-load was therefore decided to be dependent on the material and size of the specimen. Consequently it was decided separately for each test program.

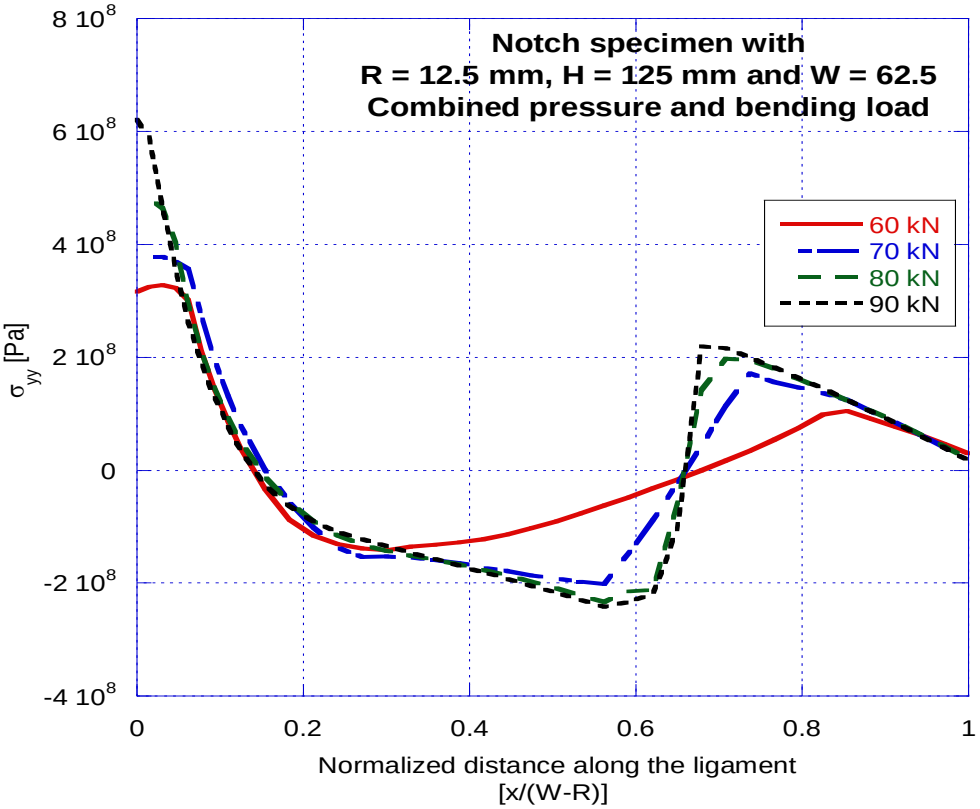

Figure 2.7: Influence on the residual stress field from the magnitude of pre-load.

2.1.4 Introducing crack before or after pre-load

In earlier works by Mirzaee-Sisan et al [5] the crack was introduced after the pre-loading. In this experimental study it was instead decided to introduce the cracks before the pre-loading. The reason for this was that uncertainties of what would happen to the residual stress field during the fatiguing of the specimen would be avoided. It was also thought to be difficult to create equally deep cracks in specimens with and without residual stresses. Since predicting the fatigue loading necessary for specimens containing residual stresses can give rise to errors. Furthermore if the crack is introduced after the pre-loading a plastic wake is created along the growth path of the crack as can be seen in Figure 2.8. If the crack is introduced before the pre-loading this is avoided.

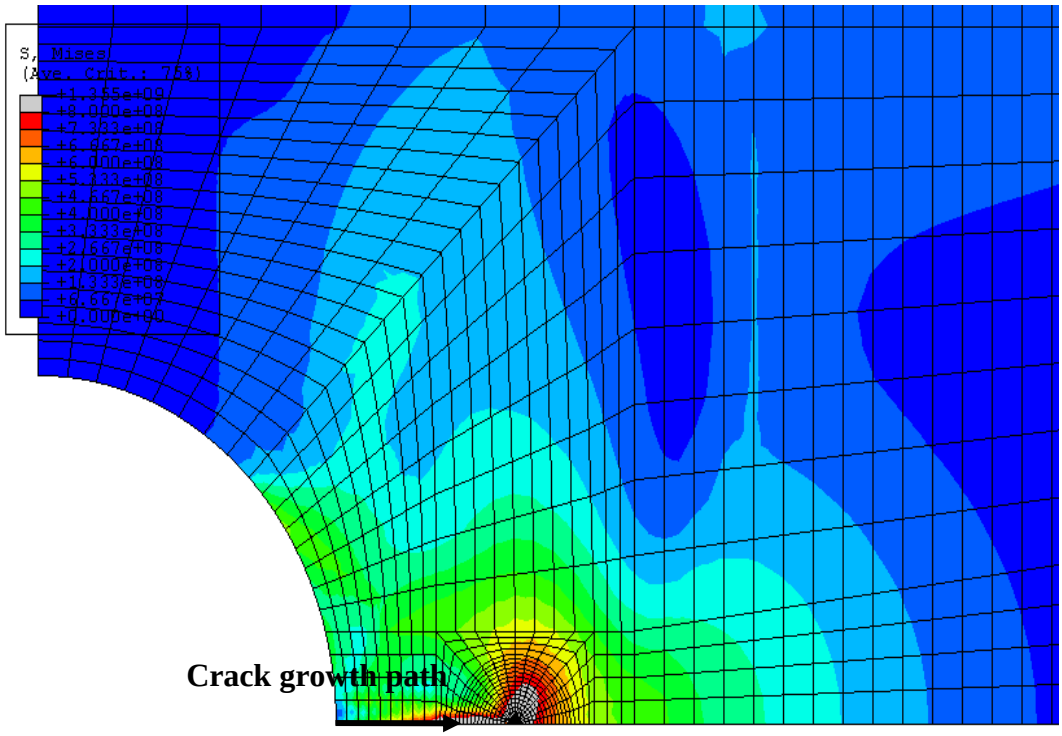

Figure 2.8: Contour plot of von Mises stress with crack introduced, after pre-loading, by sequentially releasing nodes.

2.1.5 Crack depth

The crack depth was shown to influence the size of the tensile part of the residual stress field in front of the crack tip. A shallower crack gave a larger tensile residual stress field. But at the same time a shallow crack introduces constraint effects. Since the purpose of the experiments was to examine the influence of the residual stresses, other influencing factors on the crack initiation such as constraint would cause difficulties in interpretation of the test results. For this case there were two competing effects as can be seen in Figure 2.9.

Thus, it was decided to go the middle way to allow for some constraint effects. A deep crack would lead to a highly constrained specimen and the constraint effect would be small but it would also lead to a small tensile residual stress field. A crack depth depending on the width of the specimen was decided to $a = 0.35W$.

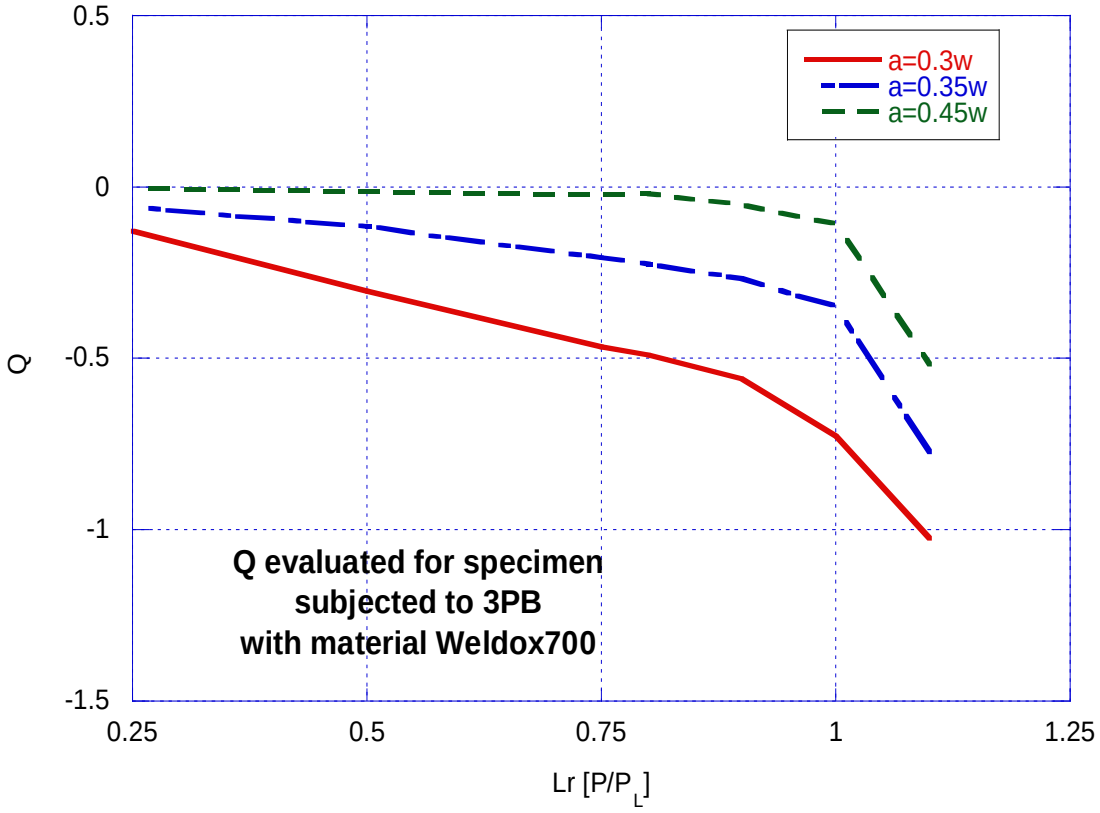

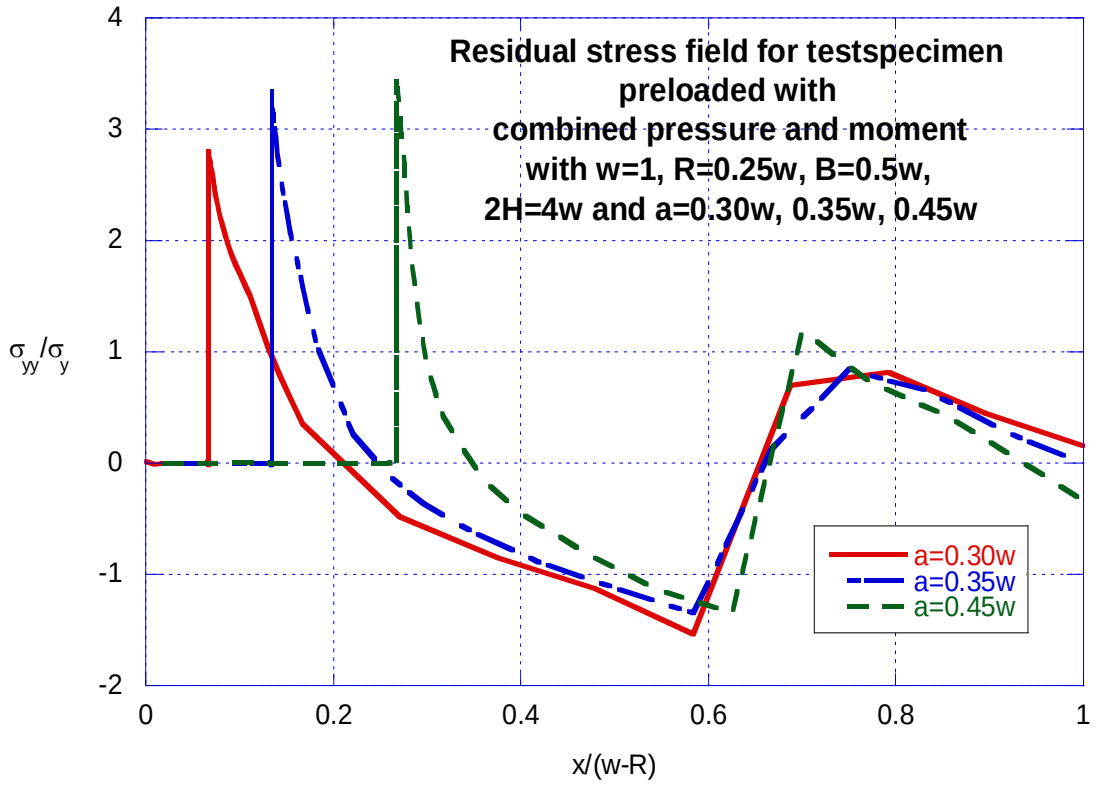

Figure 2.9: Graphs showing the effect of crack depth on constraint for specimens without residual stresses and the effect from the crack depth on the residual stress field.

2.1.6 Effect of material parameters

The effect of hardening and yield strength of the material was also investigated. The results showed a insignificant effect from both yield stress and hardening on the size of the tensile residual stress field, but it showed effects on the magnitude. From these results it was decided that the material did not influence the size of the tensile residual stress field and therefore in respect of this the material choice was not governed by the size of the residual stress field. The material choice was however very important in respect to the aim to get initiation at high primary loads.

2.2 Specimen geometry

A base test specimen geometry was chosen were all geometric parameters were dependent on the width of the specimen *W*. The dependencies for the geometric parameters of *W* were decided from the influence they had on the residual stress field. Below the base specimen is shown in Figure 2.10 together with the different dimensions and their dependency on *W*.

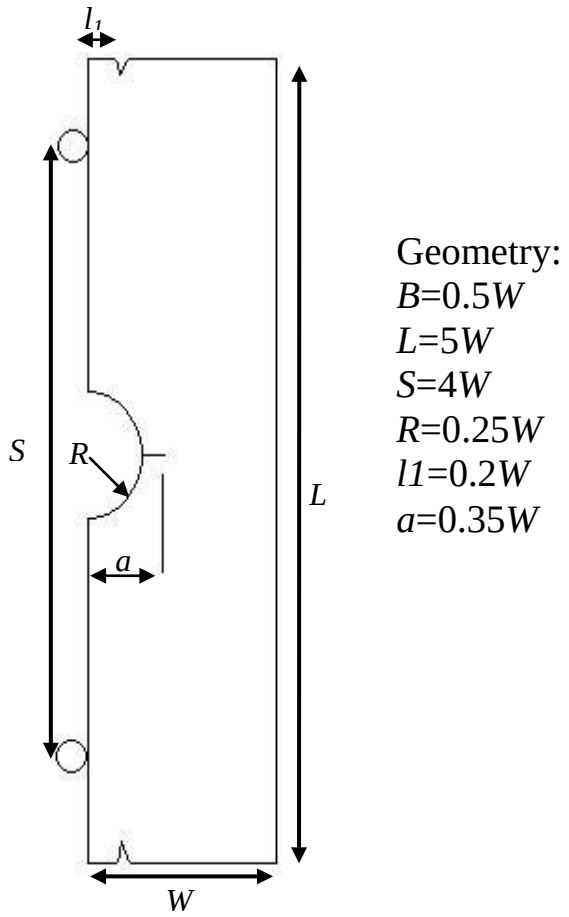

Figure 2.10: Base geometry of test specimen.

The specimen width *W*, was then used to control at which level of primary load crack initiation would occur. One goal for the experiments was to get crack initiation at high primary loads. The specimen width *W* for the different test programs was chosen to appropriate values for the used materials for initiation at L_r to cover a range between 0.9 and 1.1. To choose a suitable *W* value FE-analyses were used were initiation was predicted at around J_{Ic}. In Figure 2.11, the value of *Kr* ($Kr=(J/J_{Ic})^{1/2}$) is plotted against L_r ($L_r=P/P_L$) for the material Weldox 700 and A533B with different specimen widths. These curves were governing in deciding the width of the specimens in the test programs.

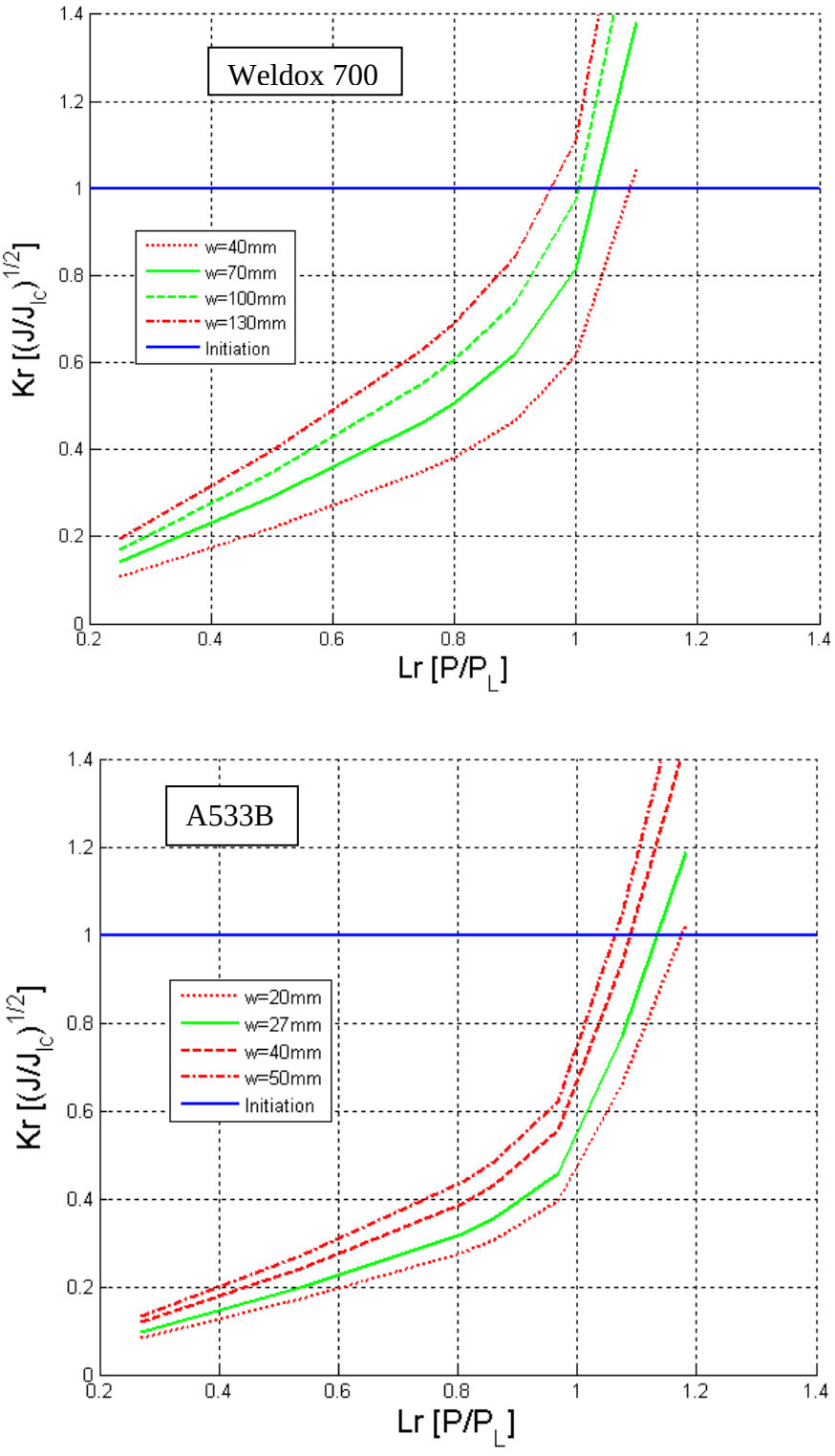

Figure 2.11: Curves used in deciding the specimen size.

3 EXPERIMENTAL SETUP AND MATERIALS

All the experimental tests were performed at the department of solid mechanics at KTH. Several tests were performed for the different materials to understand and correctly model the materials. Below is a list of all the tests that were performed to characterize the materials.

- Uniaxial tensile tests at room temperature for Weldox 900, Weldox 700 and A533B
- Uniaxial compression tests at room temperature for Weldox 900 and Weldox 700 30 mm plate
- Cyclic tests for Weldox 700 and A533B
- Standard *J*-R tests for Weldox 900, Weldox 700 and A533B
- Standard *J*-R test for Weldox 700 with virgin and pre-compressed material (0%, 1.5% and 3% total compressive strain)

The *J*-R tests on virgin and pre-compressed material were conducted to examine any effects of the pre-compression of the material without any effects from residual stresses. These analyses did not show any significant effects from the compressed material compared with the virgin material.

Based on the results from the pre-study, three test programs were conducted using two materials. In these test programs two different materials were used Weldox 700 and A533B. The reason for using Weldox 700 instead of Weldox 900 was the effect the material fracture toughness and yield strength had on the needed size of the test specimen. Since both Weldox 700 and 900 show low hardening behaviour there was a need for a material with high hardening to be able to achieve fracture for Lr>1. For this purpose A533B was chosen. The three test programs were chosen to cover crack initiation load of L_r between 0.9 and 1.1. This was controlled with the width of the specimens. Below the three different test programs are described.

Test program 1, crack initiation at L_r=0.9:

- Two *J*-R test specimens with notch (without residual stresses)
  - Material: Weldox 700 60 mm plate
  - Geometry: W=100 mm, B=0.5W, L=5W, S=4W, R=0.25W, l_1=0.2W, a=0.35W
  - Load: 3PB
- Four *J*-R test specimen with notch (with residual stresses)
  - Material: Weldox 700 60 mm plate
  - Geometry: W=100 mm, B=0.5W, L=5W, S=4W, R=0.25W, l_1=0.2W, a=0.35W
  - Load: Pre-load (P=954 kN) and 3PB

Test program 2, crack initiation at L_r=1.0:

- Two *J*-R test specimens with notch (without residual stresses)
  - Material: Weldox 700 60 mm plate
  - Geometry: W=70 mm, B=0.5W, L=5W, S=4W, R=0.25W, l_1=0.2W, a=0.35W
  - Load: 3PB
- Four *J*-R test specimen with notch (with residual stresses)
  - Material: Weldox 700 60 mm plate
  - Geometry: W=70 mm, B=0.5W, L=5W, S=4W, R=0.25W, l_1=0.2W, a=0.35W
  - Load: Pre-load (P=516 kN) and 3PB

Test program 3, crack initiation at L_r=1.1:

- Four *J*-R test specimens with notch (without residual stresses)
  - Material: A533B
  - Geometry: W=27 mm, B=0.5W, L=5W, S=4W, R=0.25W, l_1=0.2W, a=0.35W
  - Load: 3PB
- Six *J*-R test specimen with notch (with residual stresses)
  - Material: A533B
  - Geometry: W=27 mm, B=0.5W, L=5W, S=4W, R=0.25W, l_1=0.2W, a=0.35W
  - Load: Pre-load (P=55 kN) and 3PB

3.1 Pre-loading

To introduce the residual stresses in the test specimens a pre-loading was carried out on the specimens consisting of a combination of compression and bending as described earlier in chapter 2.1. In Figure 3.1 the experimental setup for the pre-loading is shown.

Figure 3.1: Experimental setup of pre-loading of test specimen.

The magnitude of the pre-load for each test program was decided by using FE-analysis. The magnitude of the pre-loading was high enough to create a residual stress field with a large enough tensile region in the front of the crack tip. During the pre-loading the load and *CMOD* (Crack Moth Opening Displacement) were recorded to be compared with the FE-analysis. This was done to verify the FE-model. In Figure 3.2 such a comparison is shown for a specimen from test program 3.

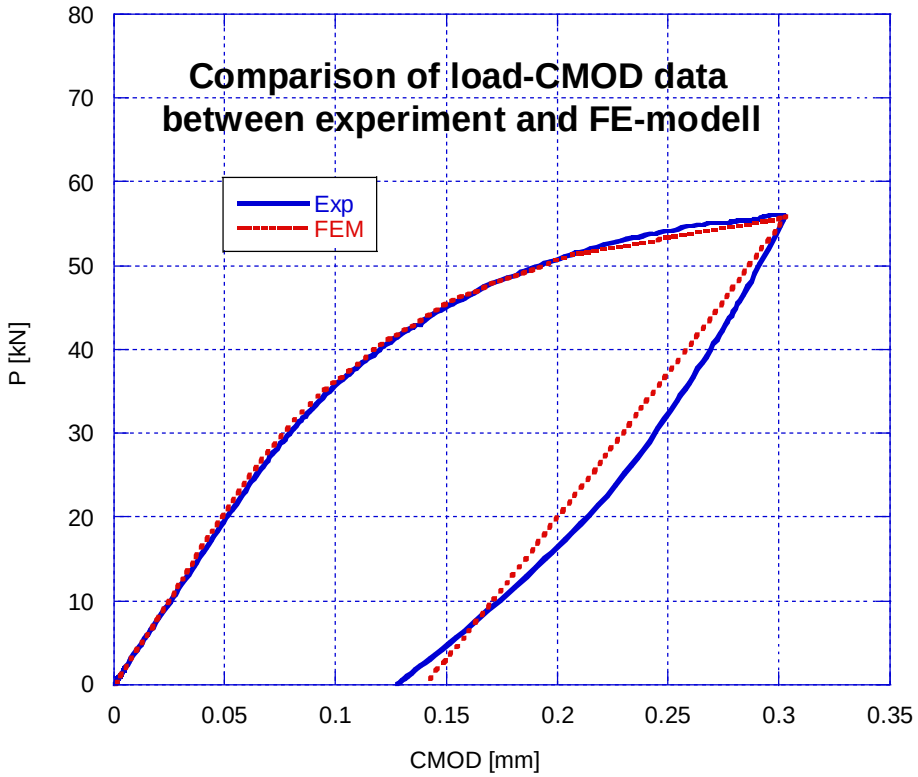

Figure 3.2: Comparison of experimental results and results from a FE-modell.

3.2 Fracture testing

The fracture tests were conducted similar to standard *J*-R testing. All specimens were loaded in 3PB during the fracture testing. The experimental setup is shown in Figure 3.3.

The load, *CMOD* and *LLD* (Load Line Displacement) data were recorded during the tests. The crack growth was monitored with both compliance calculations and by colouring. Two colourings were carried out. The first was done close to crack initiation, and the second when it was certain that some crack growth had occurred. After the second colouring, the test was carried on for some more crack growth. The tests were ended with a final fatigue loading in order to obtain four different crack fronts on the crack surface, as can be seen in Figure 3.4. The first front is the initial crack depth, the second is the first colouring, the third is the second colouring, and the fourth is the fatigue front at the end of the testing. The values of the load, *CMOD* and *LLD* related to these colourings were recorded during each test. After the fracture testing was finished the specimen was broken up to show the crack surfaces, and also to measure the different crack fronts.

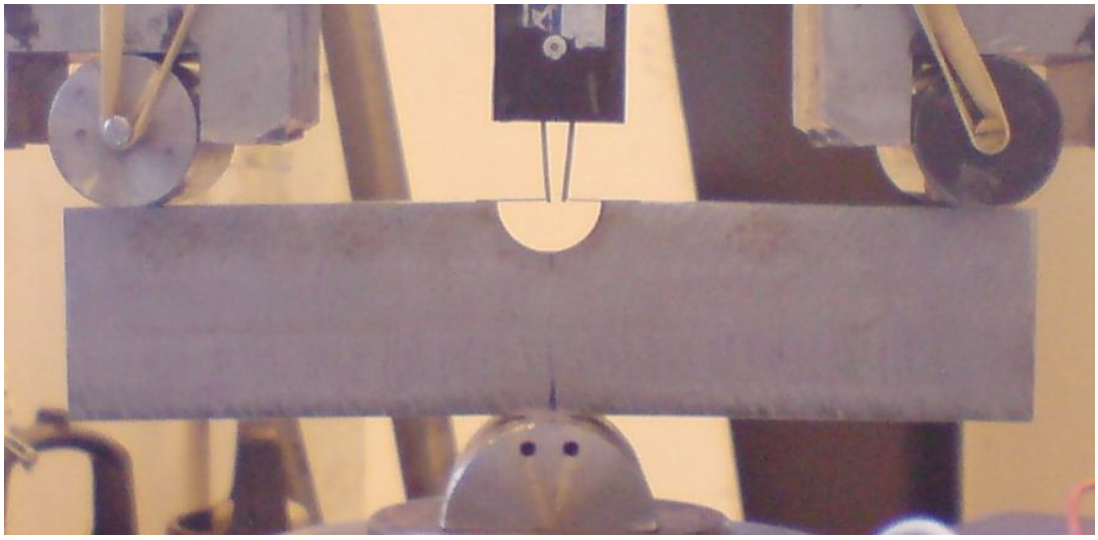

Figure 3.3: Experimental setup for fracture testing in 3PB.

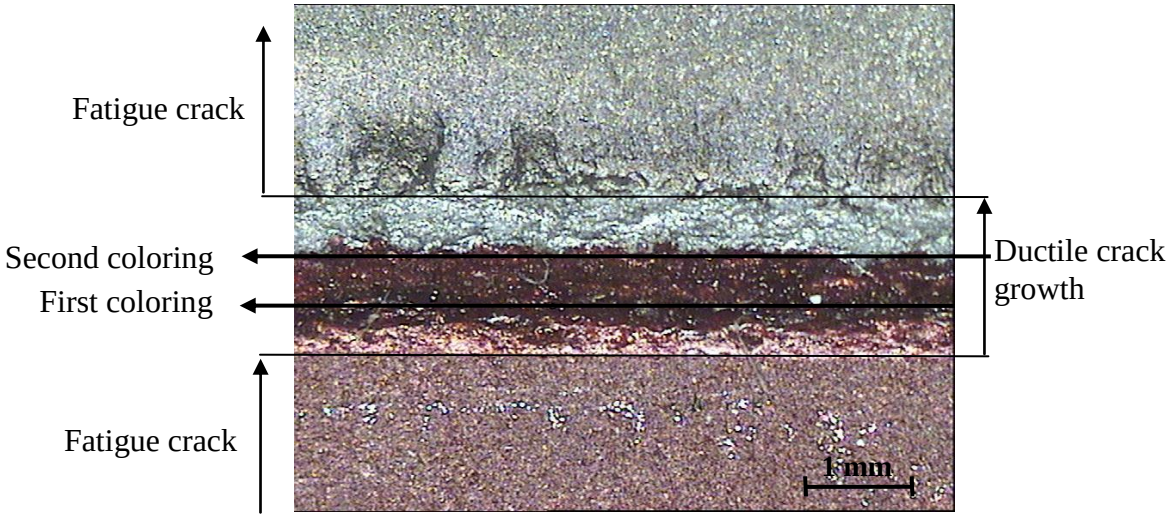

Figure 3.4: Picture of middle section of the crack surface from a test specimen, showing the different crack fronts created by colouring and fatigue loading.

4 EVALUATION OF THE EXPERIMENTAL RESULTS

Since the specimens are not standard fracture specimens, new modified methods for evaluating the experimental results were needed. The method developed for calculating the crack growth from the compliance and the *J*-integral is very similar to those found in the ASTM E 1820 standard [10]. The crack growth during the experiments was monitored by two separate methods. One method used unloading to calculate the compliance, which gives the crack depth. The second method used colouring of the crack surface which could be measured after the experiments were finished. Two separate evaluation procedures were developed to calculate the *J*-integral. Both these procedures used the load, *CMOD* data and the measured crack growths by compliance and colouring. One of the methods used only the experimental data to calculate the *J*-integral, while the other method also used FE-analyses. The experimental data were also used to verify the material models developed from the material testing.

4.1 Material characterization

Two different materials, Weldox 700 and A533B, were used during the experimental programs. Since FE analyses were used in the evaluation of the experimental results, the materials needed to be correctly modelled. To develop the material models, the results from the uniaxial tensile tests and the cyclic tests were used.

4.1.1 Weldox 700

For the Weldox 700 material an elastic-plastic material model with combined nonlinear kinematic and isotropic hardening was used. The reason for the use of this more complicated material model was that the effect on the material from the pre-loading could not be captured by a linear elastic multi linear plastic material model with isotropic hardening. To model the material, the inbuilt material model for combined non linear kinematic and isotropic hardening in ABAQUS [9] was used. This material model is based on the work of Lemaitre and Chaboche [11]. The constitutive law of the model used by ABAQUS consists of two parts as described below.

One kinematic part describing the translation of the yield surface in the stress space by the back stress α. In the material model used the temperature dependencies where omitted. The hardening law for each back stress is described by,

$$\dot{\alpha}_k = C_k \dot{\bar{\varepsilon}}^{pl} \frac{1}{\sigma^0}(\sigma - 1) - \gamma_k \alpha_k \dot{\bar{\varepsilon}}^{pl} + \frac{1}{C_k} \alpha_k \dot{C}_k , \tag{4.1}$$

Where the overall back stress α is computed as below,

$$\alpha = \sum_{k=1}^{N} \alpha_k . \tag{4.2}$$

Here, N is the number of back stresses and C_k and γ_k are material parameters calibrated from the cyclic test data.

The second part of the constitutive part is the isotropic hardening component describing the change in the size of the yield surface as a function of equivalent plastic strain. This evolution is described by using the exponential law,

$$\sigma^0 = \sigma|_0 + Q_\infty(1 - e^{-b\bar{\varepsilon}^{pl}}) \qquad (4.3)$$

where $\sigma|_0$ is the yield surface at zero plastic strain and Q_∞ and b are material parameters calibrated from the cyclic test data. In Table 4.1 the values for the different parameters in the material model described above are given.

Table 4.1: Material parameters used for the combined nonlinear kinematic and isotropic hardening material model for Weldox 700.

	E [GPA]	V	$\Sigma\|_0$ [MPA]	Q_∞ [MPA]	B	C_1 [GPA]	Γ_1
WELDOX 700	207.5	0.3	655	-250	220	63.0893	203.15

In Figure 4.1 the used material model is compared with the results from the cyclic test of Weldox 700.

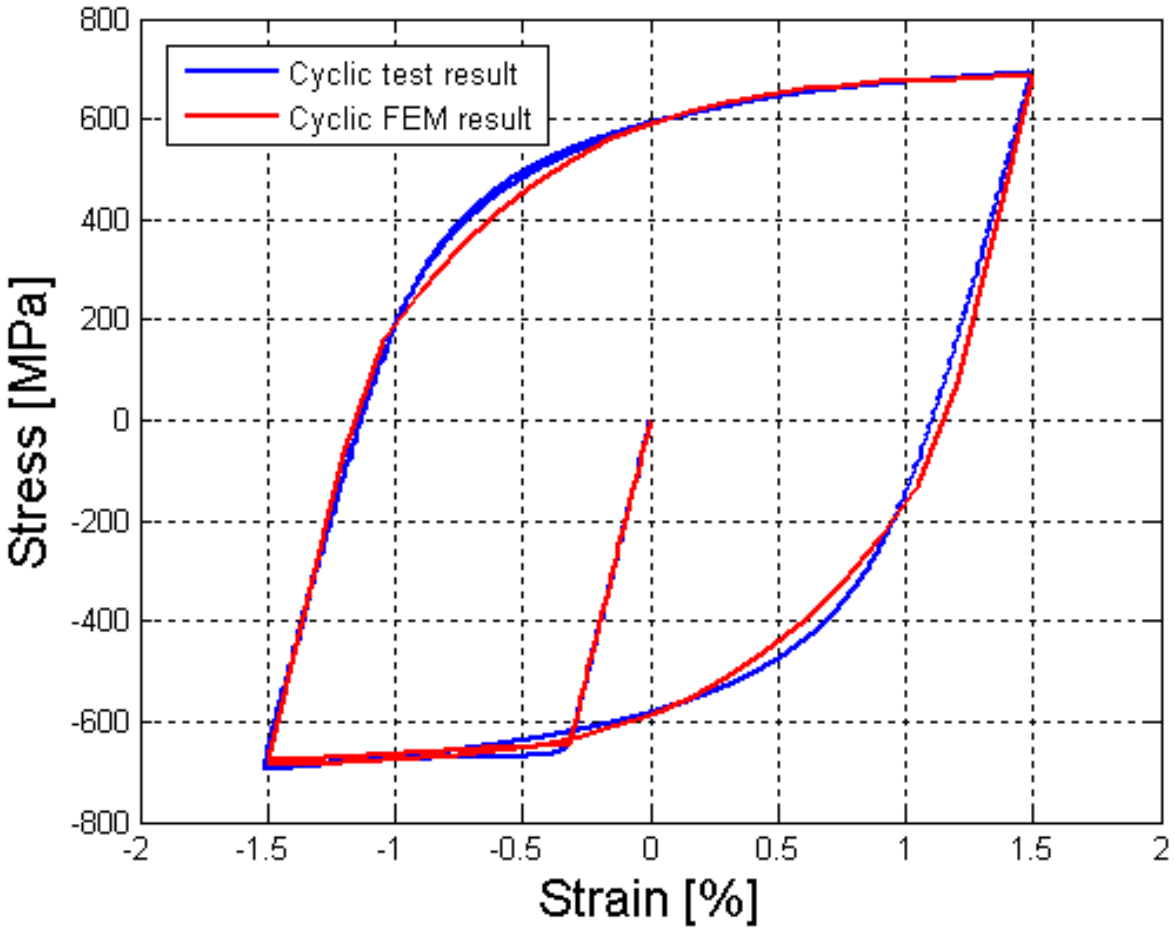

Figure 4.1. Stress strain data from cyclic test compared with FEM results for Weldox 700.

4.1.2 A533B

A533B was modelled with two different material models, one elastic multilinear plastic model with isotropic hardening and one with kinematic hardening. Both these material models are inbuilt in ABAQUS [9]. The multilinear kinematic material model is not mentioned in the ABAQUS manual [9]. Further description of this material model is given in [12]. In Figure 4.2 the stress strain curves from a uniaxial test and the modelled material are compared. The different parameters for the material properties used in ABAQUS are given in Table 4.2 below.

Table 4.2: Material parameters used in the FEM analysis for A533B.

E = 205.3 GPA	ν= 0.3
Σ [MPA]	E^{PL}
471.2	0.0
480.3	0.010767
489.0	0.014855
507.6	0.018494
539.4	0.026489
576.0	0.038381
601.1	0.049059
621.4	0.060270
643.9	0.077280
657.7	0.091113
669.0	0.10652
683.6	0.13425
721.0	0.24436
809.0	0.44844

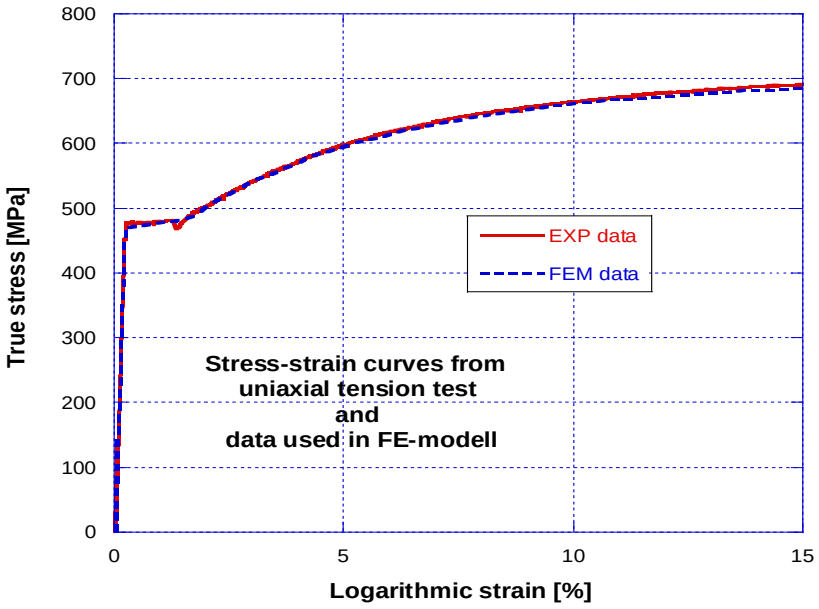

Figure 4.2: True stress-strain data from uniaxial tension test and data used in FE-modells for A533B.

It should be noted that the two different hardening material models gave actually very similar residual stress fields in the specimens, as can be seen in Figure 4.3.

Both material models showed no difference in the load-*CMOD* responses for the as-received specimens. But for the pre-loaded specimens some differences could be observed for high loads, as shown in Figure 4.4.

Both models did show rather good agreements with the experimental results. The isotropic material model did however show slightly better correlation to the experimental results at higher loads see Figure 4.5. From these investigations, it was decided that the isotropic material model should be used in the evaluation of the experimental results of the specimens of the A533B material.

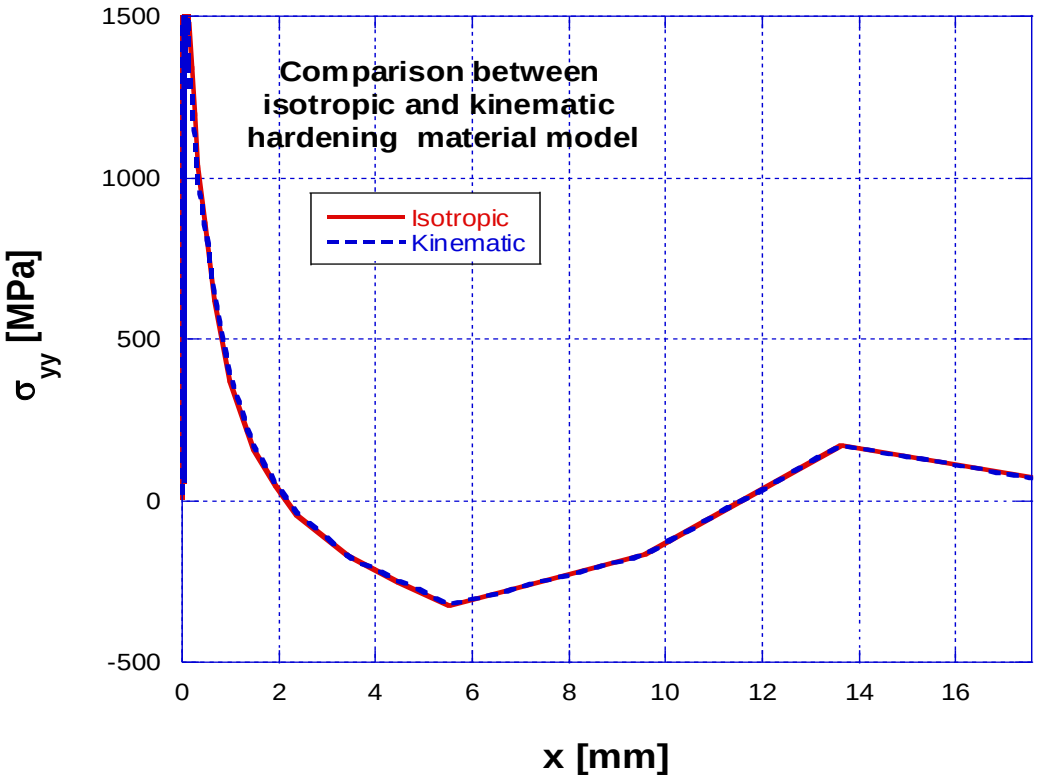

Figure 4.3: Comparison between isotropic and kinematic hardening model for the imposed residual stress filed for A533B.

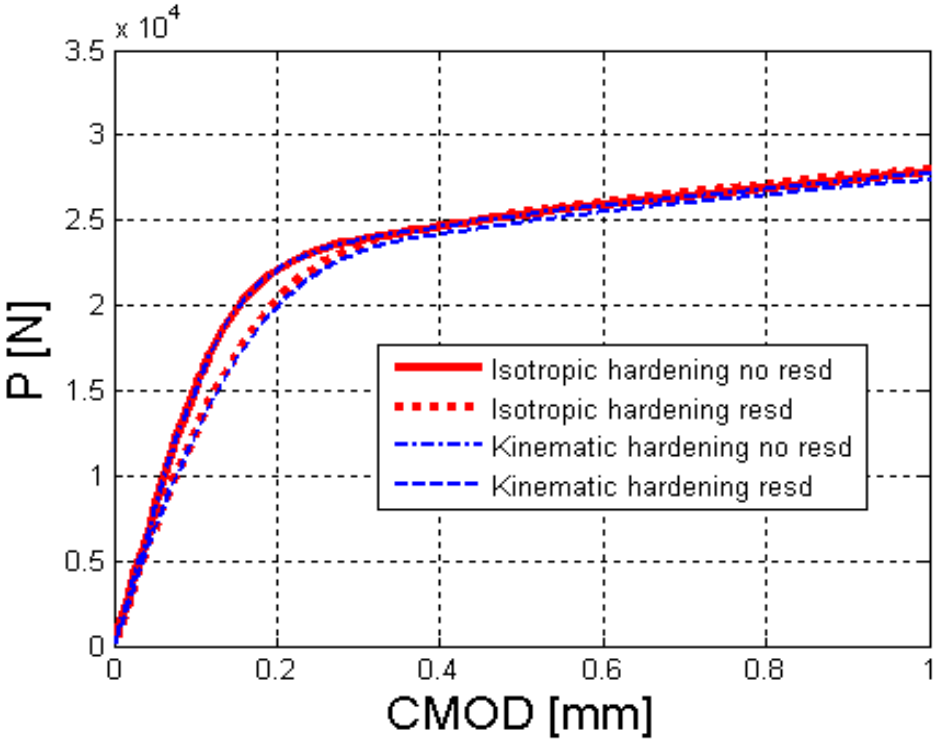

Figure 4.4: Comparison between isotropic and kinematic hardening material model in behaviour of specimens with and without residual stresses for A533B.

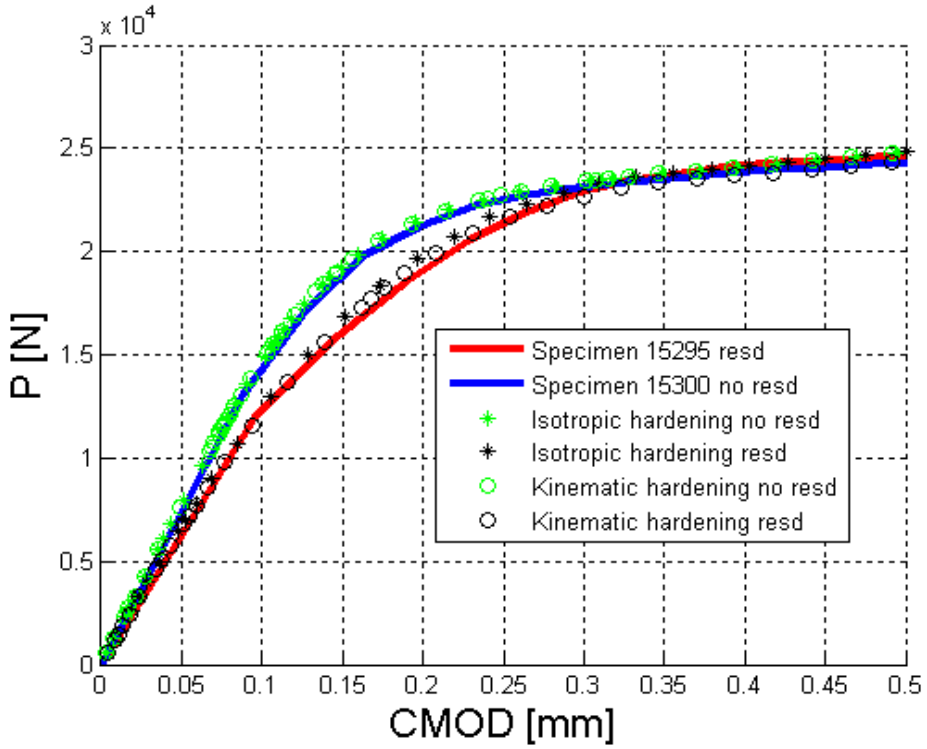

Figure 4.5: Comparison of material models to experimental results in behaviour of specimens with and without residual stresses for A533B.

4.2 Crack growth calculation

The compliance method was one of the used methods to monitor the crack growth during the tests. This method uses the correlation between the crack length and the stiffness of the specimen. When the crack grows, the stiffness of the specimen decreases and thereby the compliance increases. By measuring the compliance of the specimen during the test by small unloadings at even intervals, the crack growth can be calculated, as shown in Figure 4.6.

In ASTM E 1820 there are several expressions for the compliance function to calculate the crack growth for different standard fracture test specimen. But since the developed specimens in this study do not correlate to any of the standard specimens, a new expression for the compliance was developed. This expression could also handle eventual knife edges heights. Several elastic FE-models with varying crack depth were used to derive the parameters to the equations below.

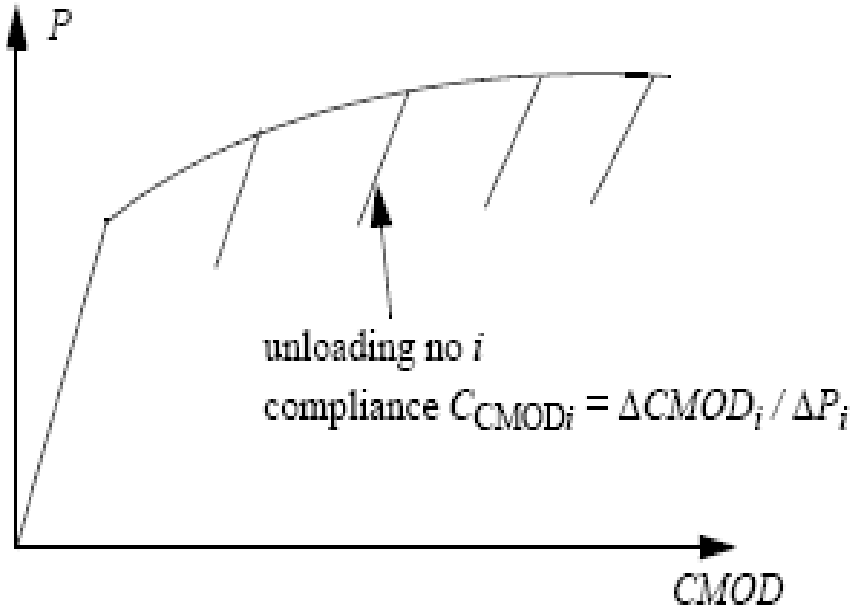

Figure 4.6: Load-*CMOD* curve with unloading were the compliance is calculated.

$$\beta_i = \alpha_i^1 + \frac{e}{W}\alpha_i^2 \qquad i = 1\ldots6 \tag{4.4}$$

$$\frac{a_i}{W} = \beta_6 + \beta_5 U_i + \beta_4 U_i^{\,2} + \beta_3 U_i^{\,3} + \beta_2 U_i^{\,4} + \beta_1 U_i^{\,5} \tag{4.5}$$

Where a is the crack depth, W specimen width, e the knife edges height defined in Figure 4.7, the constants α given in Table 4.3, and U_i from Equation (4.6).

$$U_i = \frac{1}{\left(\frac{BWEC_{CMOD,i}}{S/4}\right)^{1/2} + 1}. \tag{4.6}$$

Where *B, W, S* are defined in Figure 2.10, *E* is the elastic modulus and C_{CMODi} is the compliance defined in Figure 4.6.

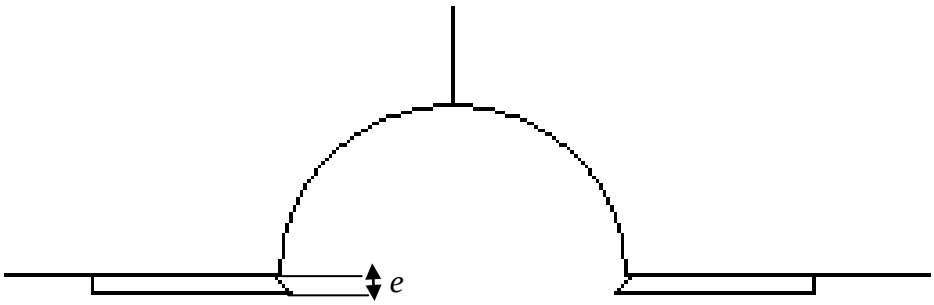

Figure 4.7: Knife edge height *e* defined as the distance between specimen and points of measurement of CMOD.

Table 4.3: Coefficients α_i in Equation (4.5).

I	1	2	3	4	5	6
A_I^1	-39249.886	33681.003	-11575.471	1993.449	-175.025	6.881
A_I^2	-245134.258	178128.945	-50672.316	6983.084	-460.379	11.104

The four different crack fronts, obtained by the colouring and fatigue loading, were measured by the nine point average method. These measured crack depths were used to calibrate the results obtained from the compliance method.

4.3 *J*-integral evaluation

Two different methods for calculating the *J*-integral were developed. The reason for developing two methods was that for the specimens with residual stresses the method using only experimental data was not considered to give reliable data at low load levels, since it did not take into account the elastic contribution from the residual stresses to the *J*-integral. Therefore a second method using FE-analyses was developed, and the first method was used to verify the second method for the specimens without residual stresses. Both of these methods are described in more detail below.

4.3.1 *J*-integral calculation from the load-*CMOD* results

The calculation of the *J*-integral from the load-*CMOD* data is very similar to the one described by Zhu et al in [13], but having different expressions due to non-standard specimens used in this study. In this method, the *J*-integral is calculated at each unloading in the experiment, and is divided in an elastic J_{el} and plastic J_{pl} part, as given in Equation 4.7.

$$J_i = J_{el,i} + J_{pl,i} \tag{4.7}$$

The elastic part J_{el} is calculated as below.

$$J_{el,i} = \frac{K_I(P_i, a_i)^2\left(1-\nu^2\right)}{E} \tag{4.8}$$

where K_I is obtained from the handbook solutions, E is the elastic modulus, ν the poisons ratio. Since the designed test specimen is not a standard specimen the K_I solutions needed to be developed. This was done by 3D elastic FE-models with different crack depths.

The plastic part J_{pl} is calculated as below.

$$J_{pl,i} = \left[J_{pl,i-1} + \frac{\eta_i}{Bb}(A_{pl,i} - A_{pl,i-1}) \right] \cdot \left[1 - \left(\frac{a_i - a_{i-1}}{b_{i-1}} \right) \right] \tag{4.9}$$

where A_{pl} is the plastic work defined by the area under the load-*CMOD* curve obtained from the experiments, η depends on a/W as described in Equation 4.10, B is the specimen thickness and $b = W-a$ is the remaining ligament of the specimen.

$$\eta_i = 4.132 - 3.101\left(\frac{a_i}{W}\right) + 2.018\left(\frac{a_i}{W}\right)^2 \tag{4.10}$$

The η factor described by equation 4.10 was determined by the use of several elastic plastic 3D FE-models where the relative error $(J_{abq}-J_{CMOD})/J_{CMOD}$ was minimised. J_{abq} is the *J*-integral value obtained from ABAQUS domain integral method while J_{CMOD} is the *J*-integral value calculated

from the same FE-model but with the developed method described earlier. The relative error between the values from ABAQUS and the load-*CMOD* method were less than one percent.

4.3.2 *J*-integral calculation with FEM and *CMOD* results

The method used for the presented *J*-integral results in chapter 5 of this report used *CMOD* and crack growth data from the experiments and *J*-integral data obtained from the FE-analyses. Through several FE-models a correlation between *CMOD* and the *J*-integral for different crack depth was derived for each specific test program and for specimens with and without residual stresses. This correlation was then used to obtain *J*-integral values at each unloading point during the test. Since the load-*CMOD* curves from the experiments did agree well with those obtained from the FE-analyses, as shown in Figure 4.8, this led to reliable results in determining of the *J*-integral.

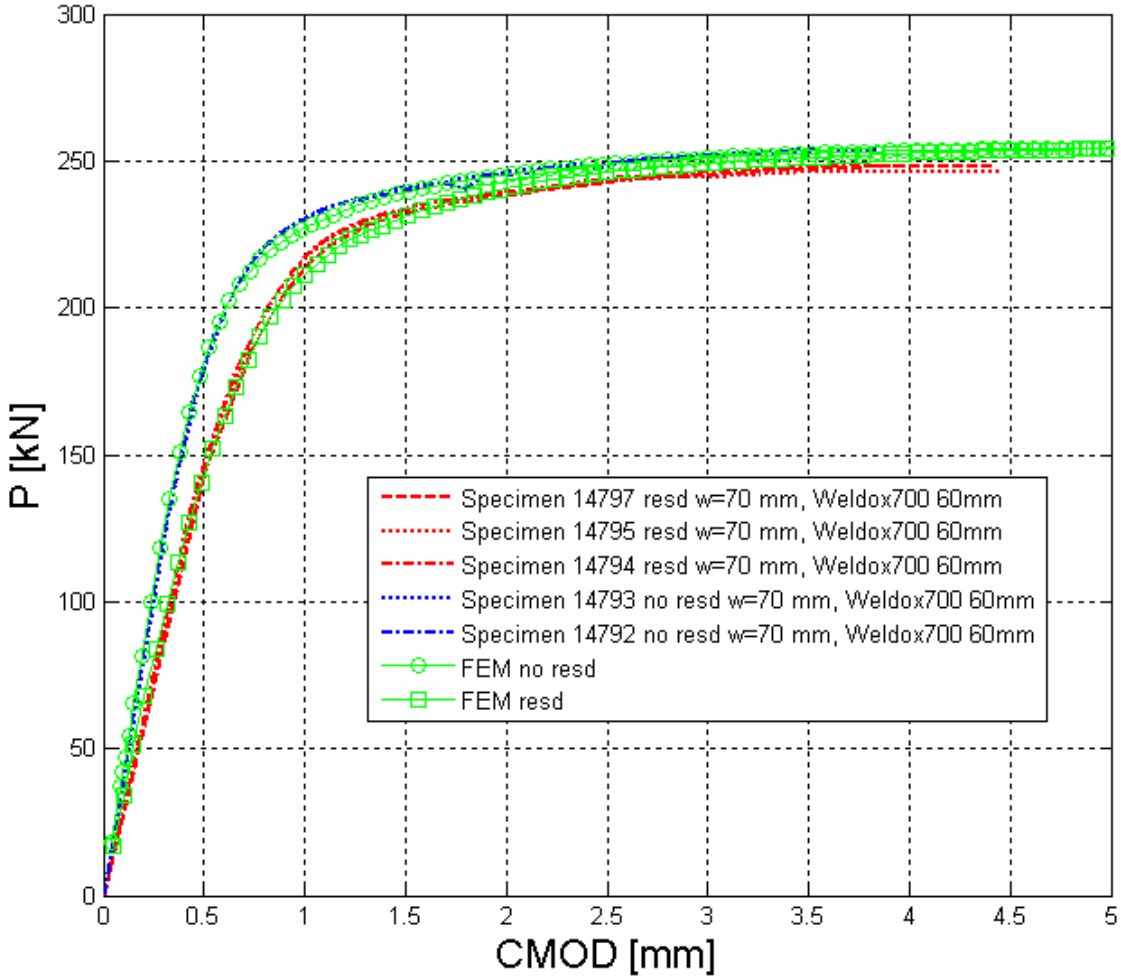

Figure 4.8: Load-*CMOD* curves for experiments from test program 2 compared with results obtained from FE-analyses.

One problem with this method is that the standard *J*-integral becomes path-dependent when residual stresses are present. This leads to uncertainties when using the standard *J*-integral in the presence of residual stresses. This has spawned considerable efforts in recent years to develop a path-independent form of *J*, where the influence of prior plastic deformation is decoupled from the standard *J*-integral and included as an additional term in the formulation. These efforts were

successful and the modified *J*-integral formulation shows path-independence under combinations of residual stresses and mechanical loading, as shown in Figure 4.9 results from Saadati [14]. The level of path dependency the standard *J*-integral show is very dependent on the individual residual stress field.

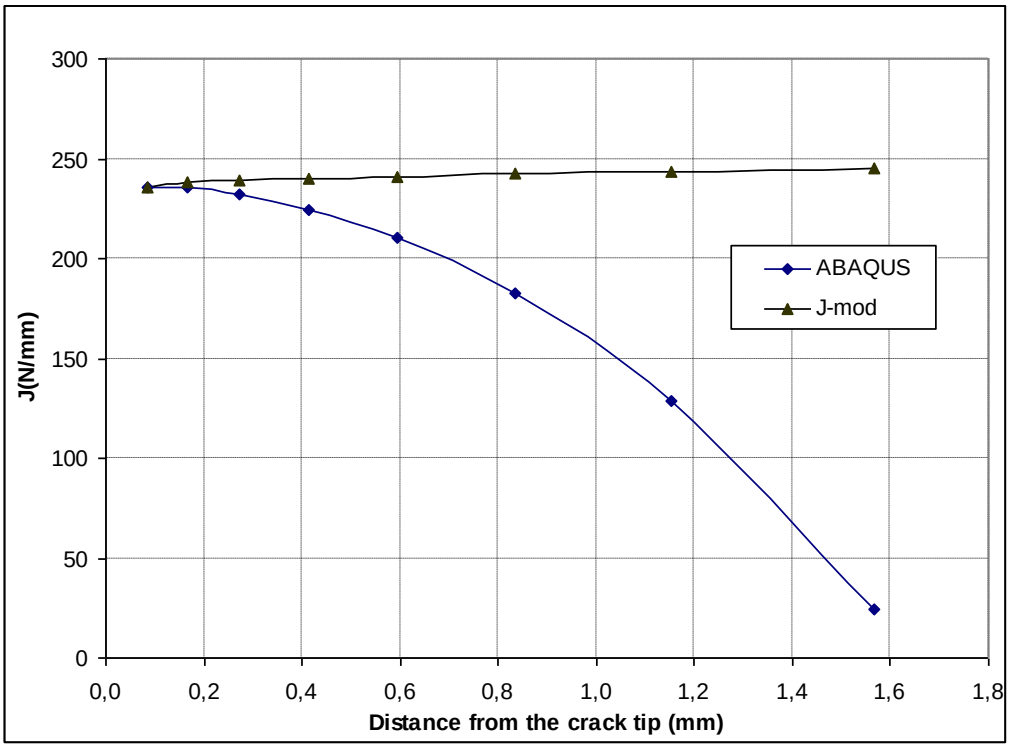

Figure 4.9: Comparison of the *J*-integral calculated by ABAQUS and by the developed script in [14], figure is obtained from [14].

Further, the modified *J* is also shown to be equivalent to the stress intensity factor *K* in cases of small scale yielding. This path-independent *J*-integral is not implemented in commercial FEM programs such as ABAQUS. But recently a script to calculate such a path independent *J*-integral have been developed by Saadati [14].

This script was however not used when deriving the correlations for specimens containing residual stresses. Studies in [14-17] on the modified *J*-integral have shown that a standard *J*-integral can also give an accurate estimate of *J*. In [14] and [15] it was shown that in an area very close to the crack tip *J* evaluated by the standard definition and by the modified definition would give almost identical results. Hence to ensure reliable *J*-integral values, the *J* values were evaluated close to the crack tip in this study. The reason for this is that the additional term in the modified definition of *J* goes towards zero as the integral is evaluated closer to the crack tip. To further ensure reliable *J* results, some of the derived *J* results were compared to results obtained with the modified definition of *J*. In Figure 4.10 this comparison is shown. In Figure 4.11 the correlation between *CMOD* and *J* for different crack depths is shown for the specimens in test program 3.

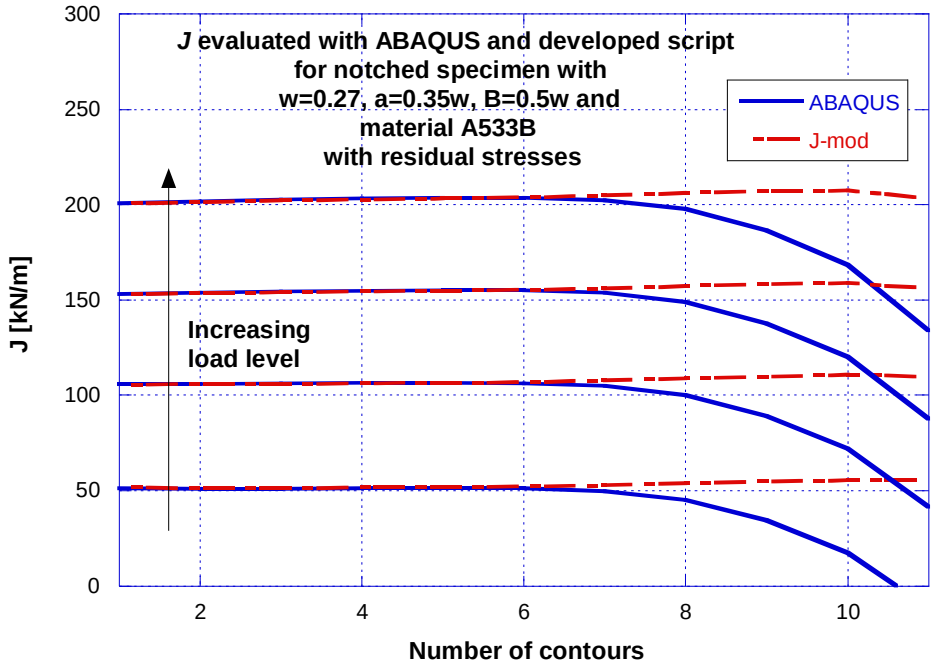

Figure 4.10: J-values calculated by ABAQUS and J-modified script for specimen from test program 3 with residual stresses at different primary load levels.

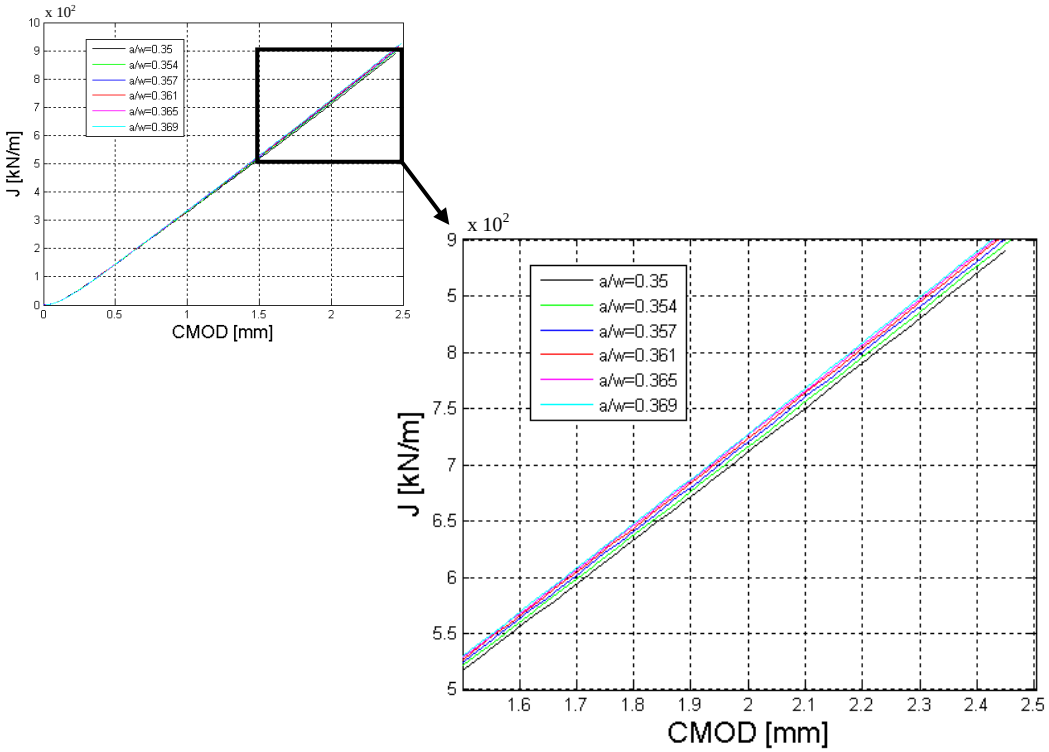

Figure 4.11: Example of *J-CMOD* curves used in evaluating the *J*-integral from the experiments.

To verify the developed methods in this study, the *J*-integral results for specimens without residual stresses were calculated using both described methods, since the method using only experimental data is not applicable for specimens containing residual stresses. In Figure 4.12 the

comparison results are shown. As can be seen, the two methods give very close results, partly due to the good correlation between the load-*CMOD* curves between the experiments and the FE-analyses.

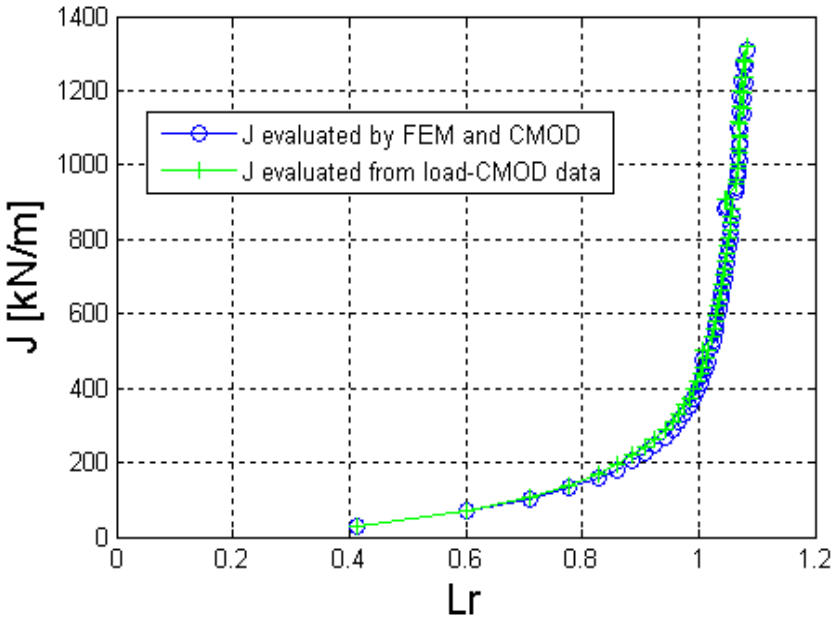

Figure 4.12: Comparison of *J* evaluated using two different methods.

4.4 Limit load definition

To decide the limit loads of the specimens used in this study, FE analyses on the different specimens were conducted. The limit load P_L used in the evaluations was defined as the load at which the whole ligament of the specimen has experienced plasticity. The models used to calculate the limit load for the different specimens used a linear elastic perfectly plastic material definition. The definition of the limit load was chosen to be consistent with the definition in the R6 method [1, 19]. The reason for this was to be able to accurately compare the experimental results with results evaluated with the R6 method. Hence the defined limit load is not representative of the actual collapse load since the hardening of the material is not accounted for. More information on calculating the limit load is given in [18]. In Table 4.4 the derived limit loads for the three test programs are presented together with the material properties used in the FE-analyses.

Table 4.4: Derived limit load for the different test program specimens and material properties used in deciding the limit loads.

	TEST PROGRAM 1	TEST PROGRAM 2	TEST PROGRAM 3
E [GPA]	207.5	207.5	205.3
V	0.3	0.3	0.3
Σ_Y [MPA]	655	655	471
P_L [KN]	460	227	24

5 RESULTS AND DISCUSSIONS

In this chapter the results from the test programs are presented. For each test program the load-*CMOD* curves, *J*-R curves and *J* versus L_r are given. The relative differences between the *J*-integral from specimens with and without residual stresses are plotted against L_r. A table for the measured crack depth from the colouring technique is also presented.

5.1 Test program 1, initiation at L_r=0.9, material Weldox 700

The influence from the residual stress field can clearly be seen in Figure 5.1 showing the load-*CMOD* curve.

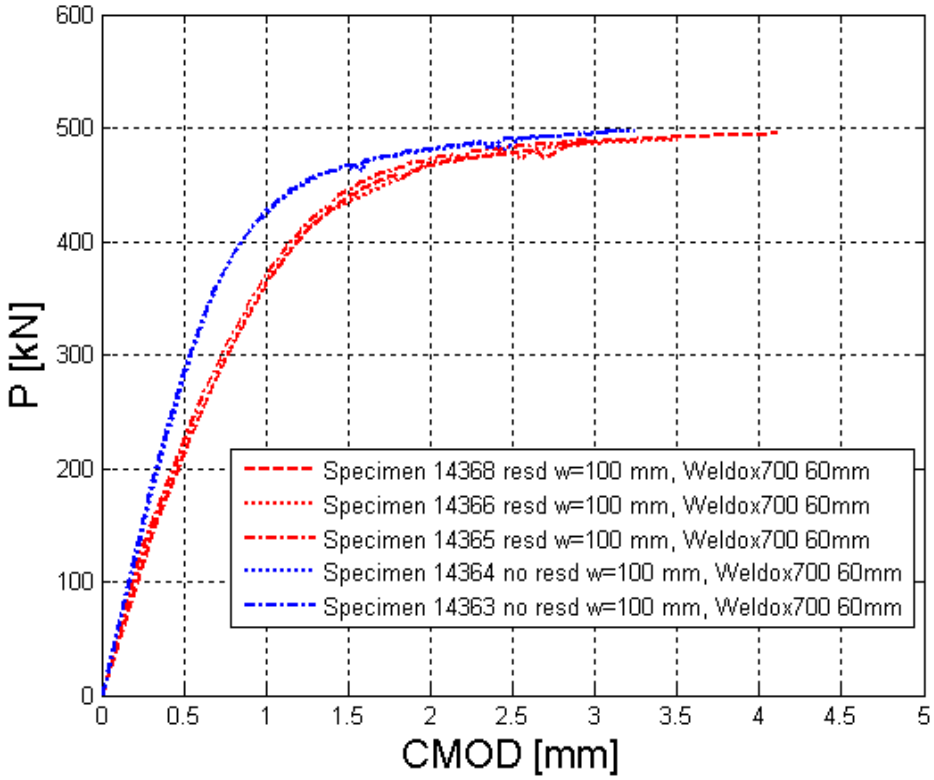

Figure 5.1: Load-*CMOD* curve from test program 1 for specimens with and without residual stresses.

In Figure 5.2 the *J*-R curves for the different specimens are given. No distinctive differences between the results from the as-received specimens and the preloaded are observed. This implies that the fracture toughness of the material is unaffected by the residual stresses and the pre-loading. This is in agreement with observations earlier by Mirzaee-Sisan et al [6] in similar experiments.

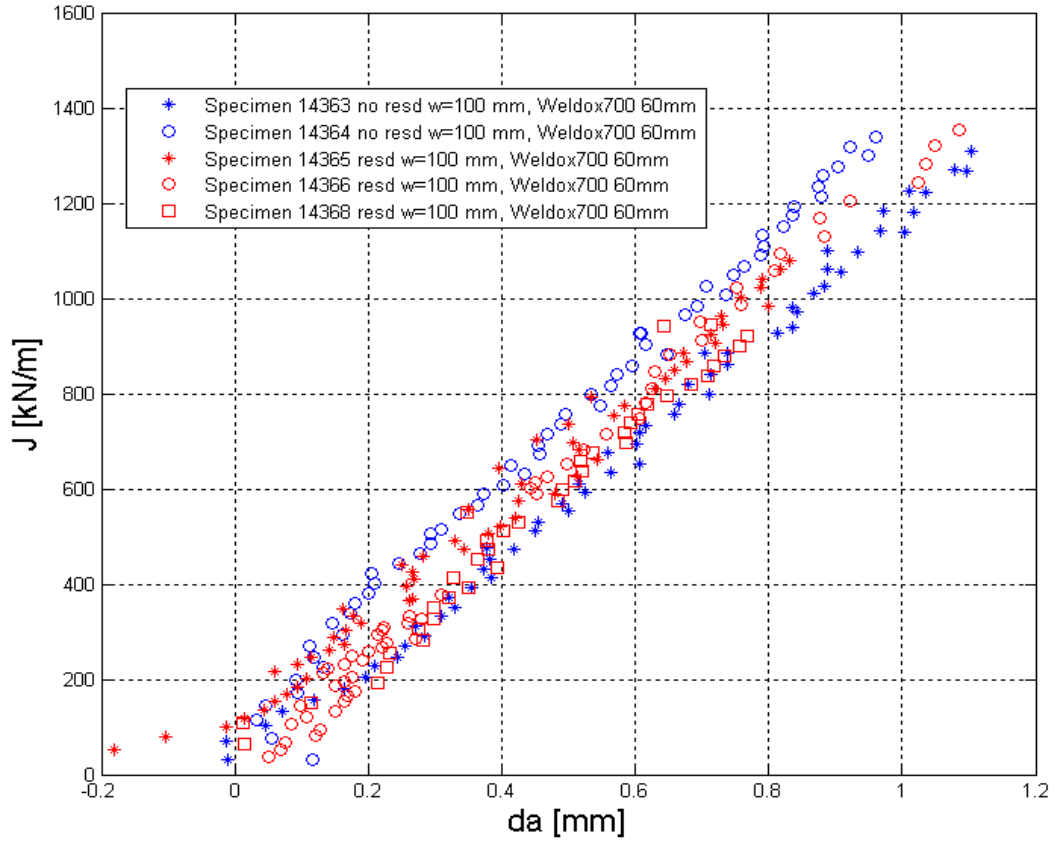

Figure 5.2: The *J*-integral results versus crack growth for specimens with and without residual stresses.

In Figure 5.3 the *J*-integral is plotted against L_r values. Here the results show a clear influence of the residual stresses on *J* for lower L_r values. But as the load level increases (higher L_r values), the influence of the residual stresses on *J* starts to diminish. The results seen in Figure 5.3 are very similar to the numerical results presented in [14]. The irregularity seen in the curves in Figure 5.3 are due to the pause of the test needed for the colouring of the crack surfaces. To compare the results from the specimens with and without residual stresses a curve fit for those with and those without residual stresses was calculated and compared. The results are presented in Figure 5.4, where the relative difference between the *J* results from specimens with and without residual stresses is plotted against L_r values. It is observed that at load levels of L_r>0.7 the relative difference in *J* becomes less than 1, and would decrease towards zero. It should be noted that the results for L_r>1 are not entirely reliable due to the steep slopes of the L_r-*J* curves, as seen in Figure 5.3 for load levels of L_r>1. This makes the results very sensitive to errors from calculating the limit loads, and thereby affecting the L_r values which in turn due to the steep slopes give a large effect on the *J* results.

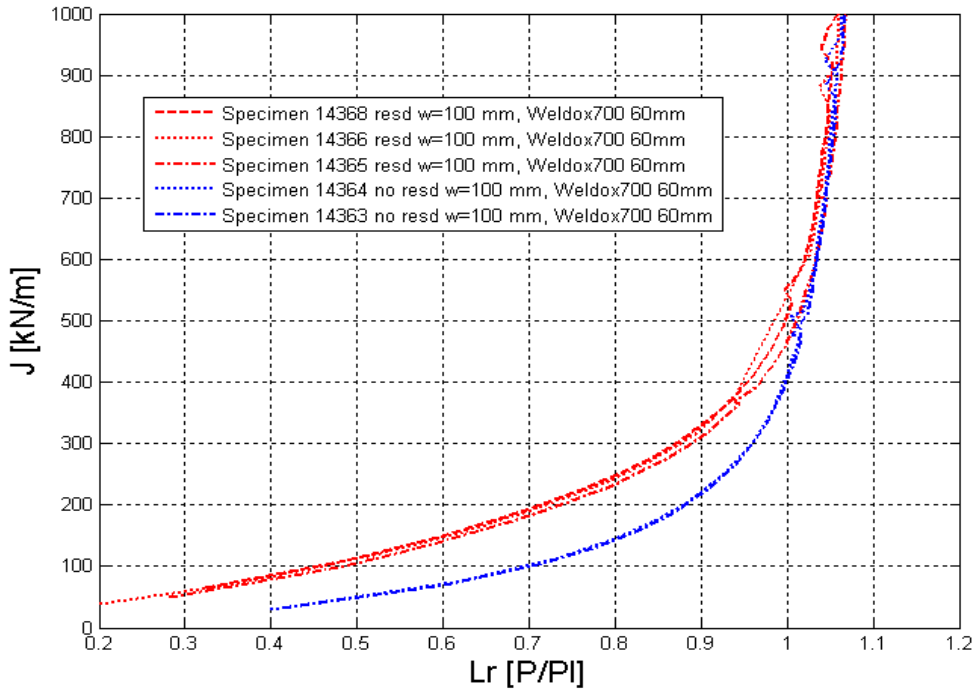

Figure 5.3: The *J*-integral results versus L_r for specimens with and without residual stresses.

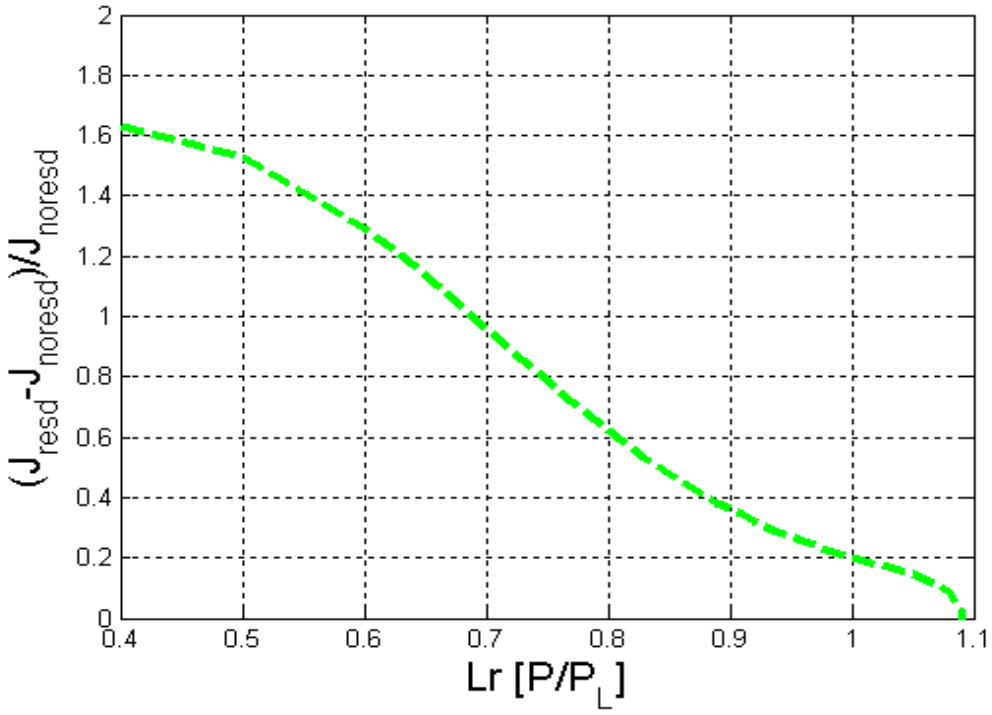

Figure 5.4: Relative difference in the *J* values in the specimens with and without residual stresses.

From the colouring of the specimens during the tests, it could also be concluded that the crack initiation occurred around $L_r \approx 0.9$. It was difficult to derive any exact difference in initiation between the pre-loaded specimens and those not pre-loaded. This is because of the difficulty in deriving the exact initiation load for the individual specimens. However at $L_r \approx 1.0$ a difference in

average crack growth could be seen related to the average L_r results between the specimens with and without residual stresses. But no difference in average crack growth could be seen between the specimens with and without residual stresses at a load level of $L_r \approx 1.05$. This implies that the effect from the residual stress field on initiation and ductile tearing at high primary loads is negligible. This conclusion can also be made from the *J*-integral results in Figure 5.3 and 5.4.

Information on the crack growth, L_r and *J*-integral values in different specimens tested in test program 1 are presented in Table 5.1 for each colouring.

Table 5.1: Evaluated results for test program 1 at each colouring.

SPECIMEN	14363	14364	14365	14366	14368
	NO PRE-LOAD	NO PRE-LOAD	PRE-LOADED	PRE-LOADED	PRE-LOADED
			FIRST COLOURING		
ΔA [MM]	0.41	0.27	0.24	0.32	0.31
J [KN/M]	477	500	368	580	545
L_R [PL/P]	1.02	1.02	0.94	1.01	1.00
			SECOND COLOURING		
ΔA [MM]	0.72	0.63	0.58	0.73	0.80
J [KN/M]	876	916	700	845	922
L_R [PL/P]	1.06	1.06	1.05	1.05	1.05

It should be noted that one of the specimens in test program 1 is removed from the evaluation. The reason for this is that the load socket used to transfer the load to the specimen during the pre-loading broke and therefore the pre-loading was ended prematurely. The specimen was pre-loaded for a second time, but it was unclear what effects this could have on the results. Therefore, it was removed from the evaluated results.

5.2 Test program 2, initiation at *Lr*=1.0, material Weldox 700

As with the results from test program 1, the influence from the residual stress field can be seen in Figure 5.5 showing the load-*CMOD* curves.

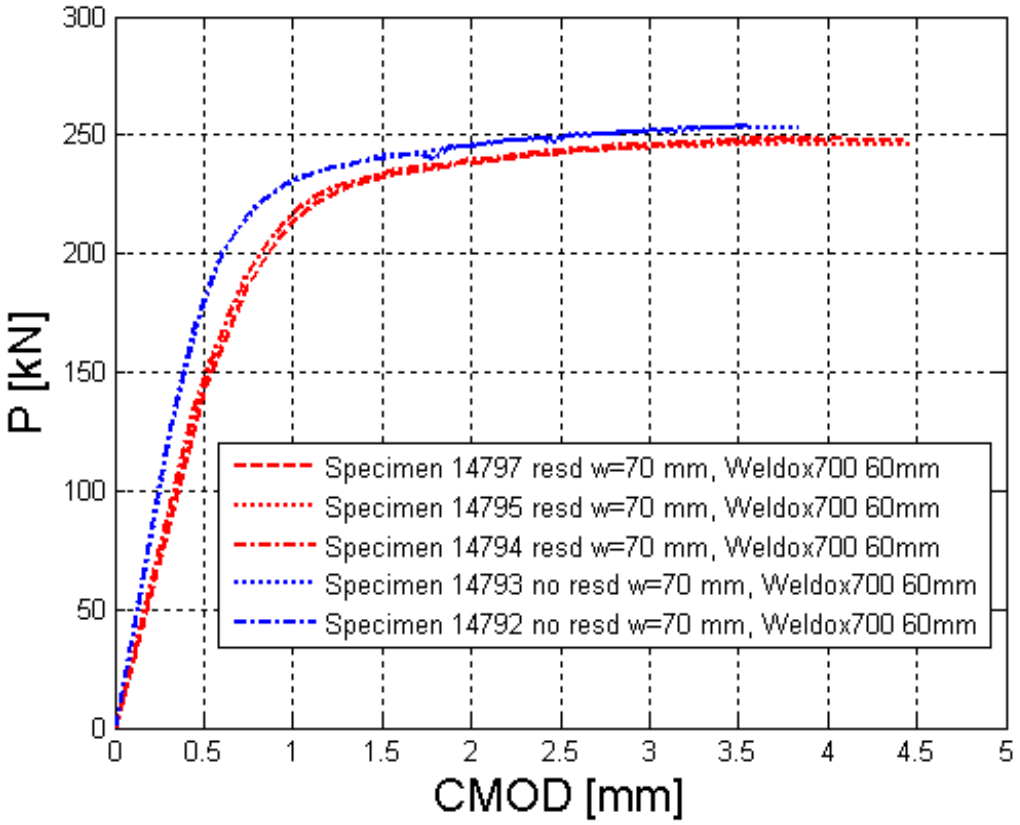

Figure 5.5: Load-*CMOD* curve from test program 2 for specimens with and without residual stresses.

In Figure 5.6 the *J*-R curves for the different specimens are presented. No distinctive differences between the results from the as-received specimens and the preloaded are observed. This implies that the fracture toughness of the material is unaffected by the residual stresses. This was also seen for test program 1, which was of the same material.

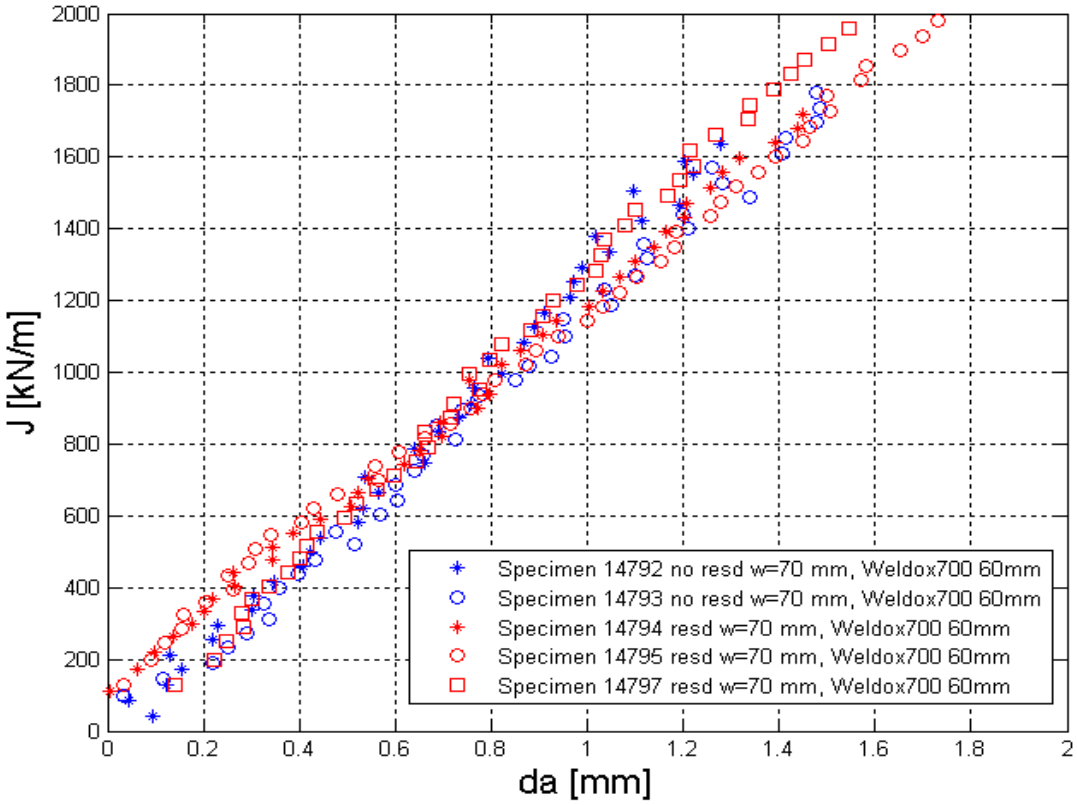

Figure 5.6: The *J*-integral results versus crack growth for specimens with and without residual stresses.

In Figure 5.7 the *J*-integral is plotted against L_r values. Here the results show a clear influence of the residual stresses on *J* for low L_r values, but as the loading increases (high L_r), the influence of the residual stresses on *J* start to diminish. For these results the two curves do not intersect as they did for test program 1. One reason for this can be that the results near the limit load are very sensitive on the defined limit load. A small change in the limit load lead value can lead to very different results of *J* in respect to L_r for high L_r values. This is due to the steep slope for the curve at high L_r values. One factor that can influence the limit load is the crack depth. Some small differences in crack depth can give differences in the limit load and these small differences can cause what is seen in Figure 5.8. This is further discussed and shown in chapter 5.3. Other factors that may influence the limit load are small changes in the experimental setup, like the distance *S* between the supports. For test program 2, the fracture testing of the specimens with residual stresses were conducted in a different test rig than those without residual stresses. This could give differences in limit load due to small differences in the experimental setup.

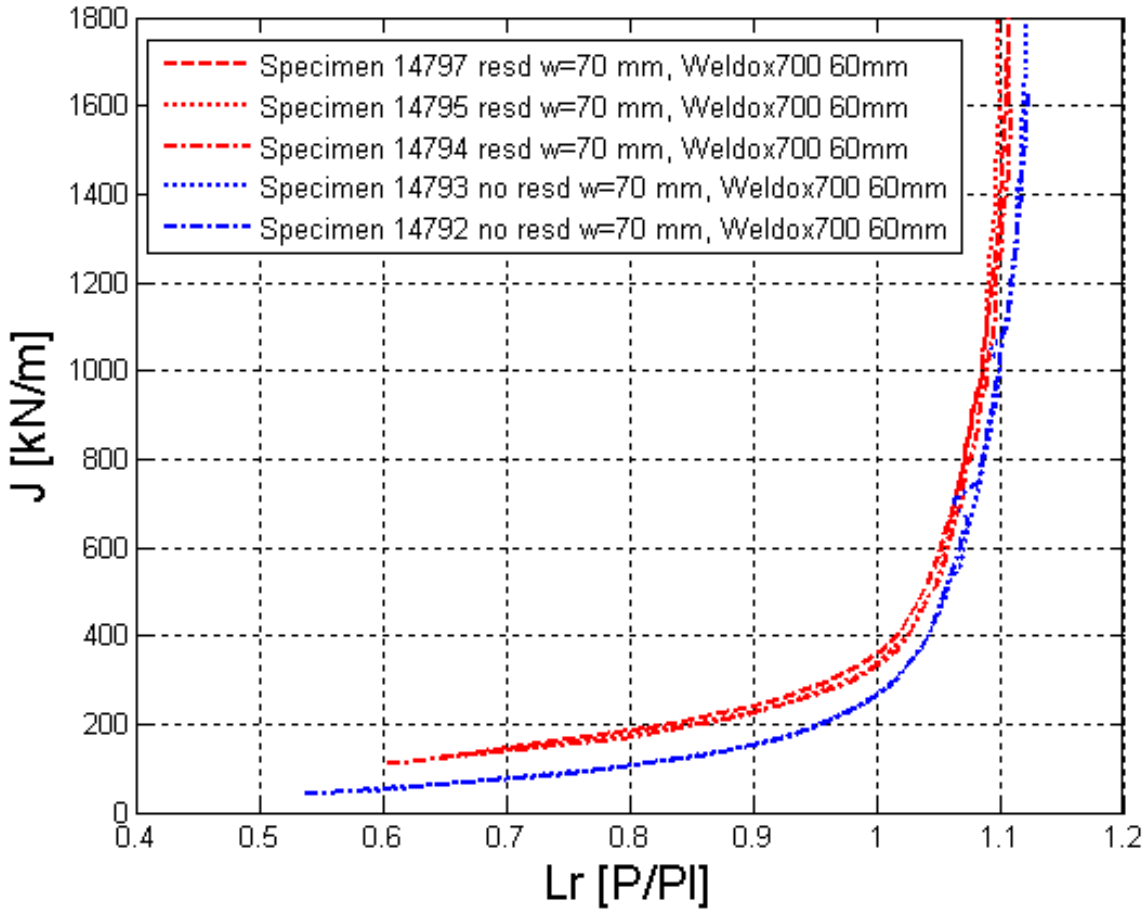

Figure 5.7: The *J*-integral results versus L_r for specimens with and without residual stresses.

In Figure 5.8 the relative difference between the *J* results from specimens with and without residual stresses is plotted against L_r values. To compare the results from the specimens with and without residual stresses a curve fit for those with and those without residual stresses was calculated and compared. The results are similar to what was observed for test program 1. The relative difference for load levels of L_r> 0.7 becomes less than 1, and is decreasing towards zero. The increase in the relative difference at L_r>1.0 is due to the sensitivity of the defined limit load as discussed above. Therefore values above L_r=1 should not be regarded as reliable.

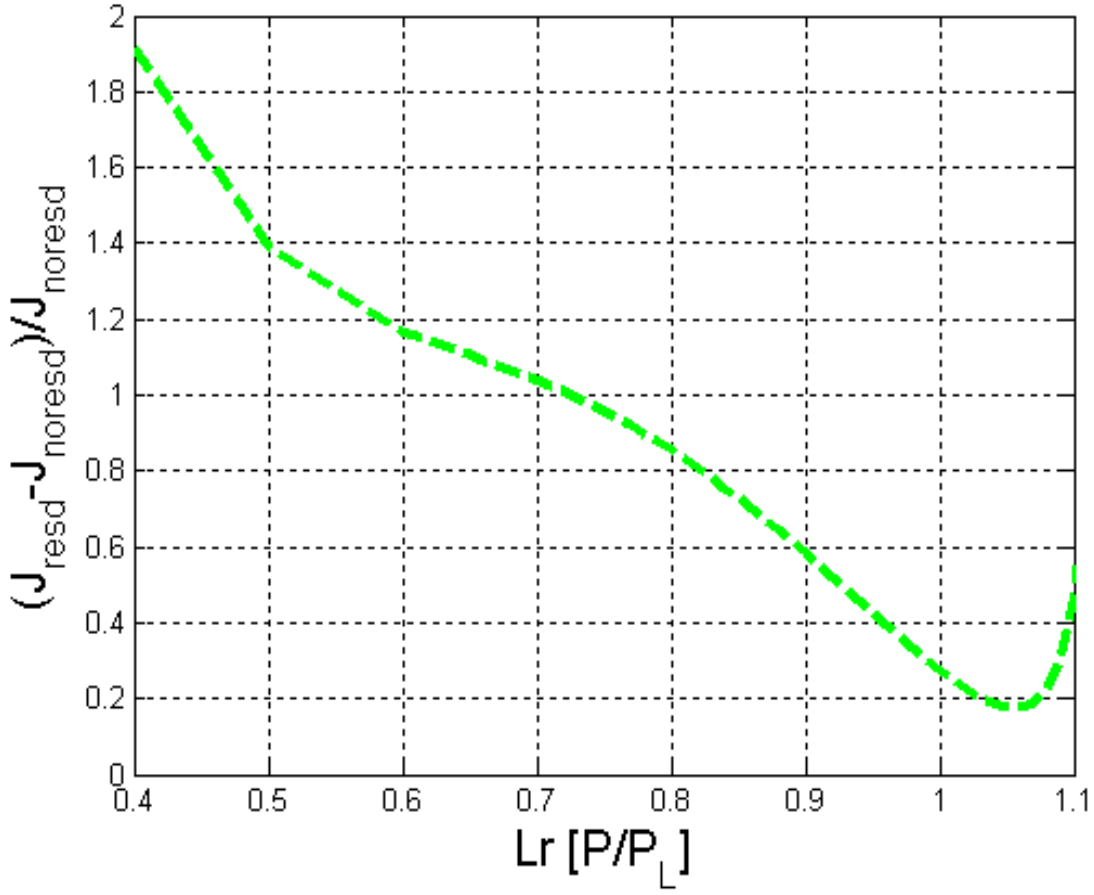

Figure 5.8: Relative differences in *J* in specimens with and without residual stresses.

From the colouring of the specimens during the tests, it was concluded that the crack initiation occurred at L_r values between 1.0 and 1.05. It was difficult to derive any difference in initiation between the pre-loaded specimens and those not pre-loaded. This is because of the difficulty in deriving the exact initiation load. However it was clear that no clear difference could be seen between the specimens with and without residual stresses in respect to crack growth at a load of $L_r \approx 1.1$. This implies that the effect from the residual stress field on initiation and ductile tearing at high primary loads is negligible. This conclusion can also be made from the *J*-integral results in Figure 5.7 and 5.8.

Information on the crack growth, L_r and *J*-integral values in different specimens tested in test program 2 are presented in Table 5.2 for each colouring.

Table 5.2: Evaluated results for test program 2 at each colouring.

SPECIMEN	14792	14793	14794	14795	14797
	NO PRE-LOAD	NO PRE-LOAD	PRE-LOADED	PRE-LOADED	PRE-LOADED
			FIRST COLOURING		
ΔA [MM]	0.15	0.46	0.45	0.37	0.43
J [KN/M]	335	530	476	473	480
L_R [PL/P]	1.03	1.06	1.04	1.04	1.04
			SECOND COLOURING		
ΔA [MM]	0.59	0.91	0.85	0.87	0.86
J [KN/M]	698	1032	942	940	955
L_R [PL/P]	1.07	1.10	1.08	1.08	1.08

It should be noted that one test within this test program is removed from the evaluation. The reason for this is that the fracture testing of the specimen was accidently prematurely ended.

5.3 Test program 3, initiation at *Lr*= 1.1, material A533B

As with the results from test program 1 and 2, the effect from the residual stress field can be seen in Figure 5.9 showing the load-*CMOD* curve, where some scatter can be seen in the results. One of the reasons for this is the small specimen size which leads to sensitivity for small changes in crack depth. A crack depth difference of 0.5 mm leads to a difference in the limit load of 6 %. In Figure 5.10 the same results are shown, but the loads are normalized with the limit load of the respective specimen depending on initial crack depth. As can be seen in Figure 5.10, the scatter is reduced if the different crack depths are considered.

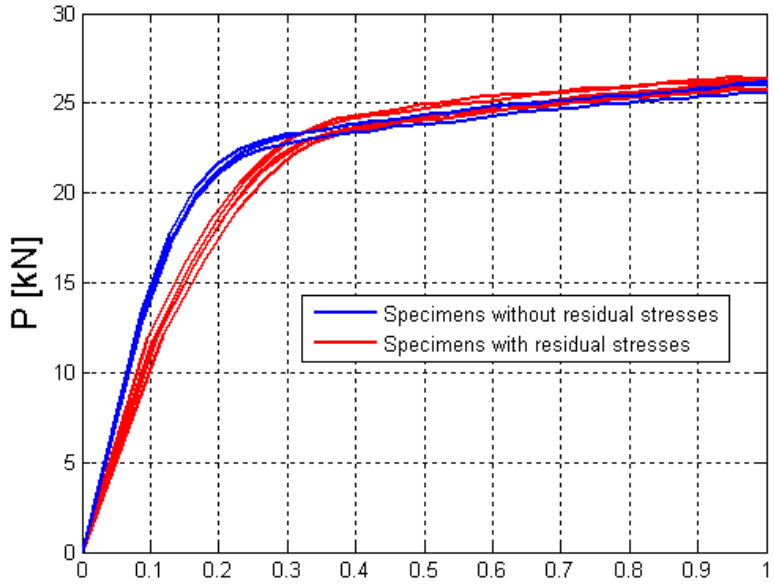

Figure 5.9: Load-*CMOD* curve from test program 3 for specimens with and without residual stresses.

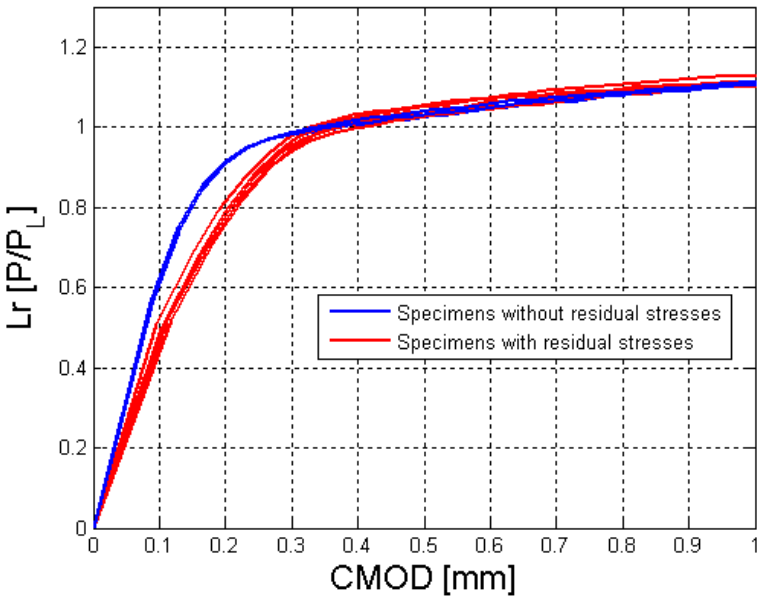

Figure 5.10: L_r-*CMOD* curve from test program 3 for specimens with and without residual stresses.

In Figure 5.11 the *J*-R curves for the different specimens are given. No distinctive differences between the results from the specimens with and without residual stresses are observed. This implies that the fracture toughness of the material is unaffected by the residual stresses. This was also seen for test program 1 and 2 which used a different material.

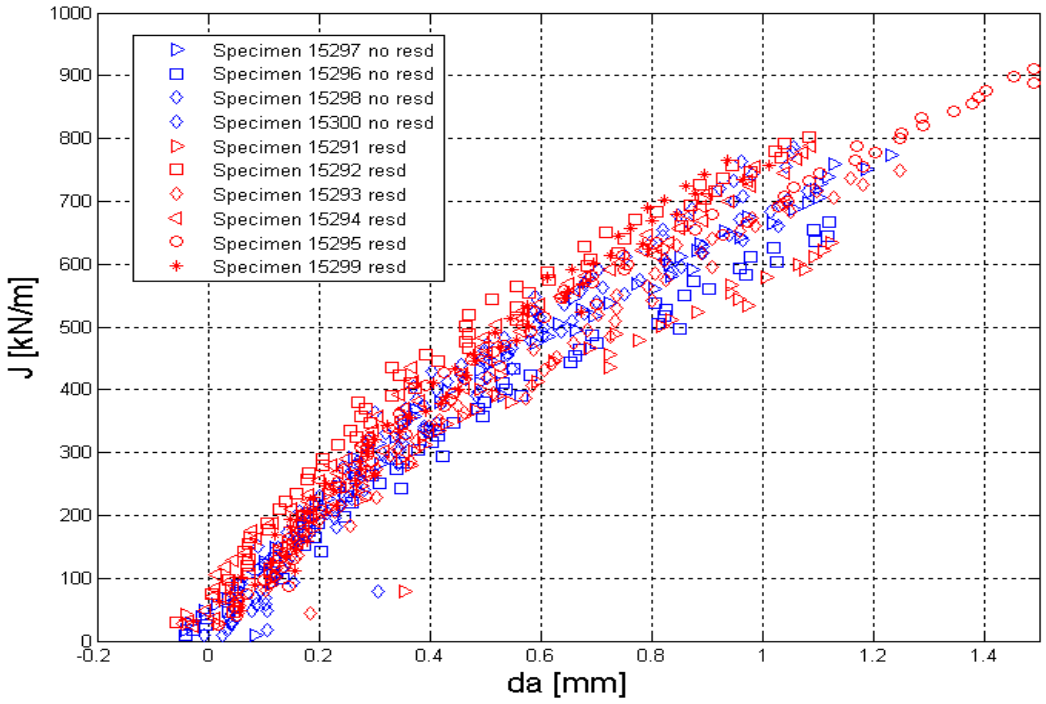

Figure 5.11: The *J*-integral results versus crack growth for specimens with and without residual stresses.

In Figure 5.12 the *J*-integral is plotted against L_r values. Here the results show a clear influence of the residual stresses on *J* for low L_r values, but as the loading increases (high L_r), the influence of the residual stresses on *J* start to diminish. In Figure 5.13 the relative difference between the *J* results from specimens with and without residual stresses is plotted against L_r values. To compare the results from the specimens with and without residual stresses a curve fit for those with and those without residual stresses was calculated and compared. Again this is similar to what are observed from the results for test programs 1 and 2. With the exception that for the specimens in test program 3 the relative difference in *J* becomes less than 1 at L_r=0.9 not 0.7, but it decreases more rapidly towards zero. Here it is also observed that the relative difference actually decreases to zero for L_r>1. Since the material A533B has a higher hardening behaviour than Weldox 700, it is not as sensitive as Weldox 700 for L_r>1, and the slope for the L_r-*J* curve for L_r>1 is not as steep as those for the other two test programs.

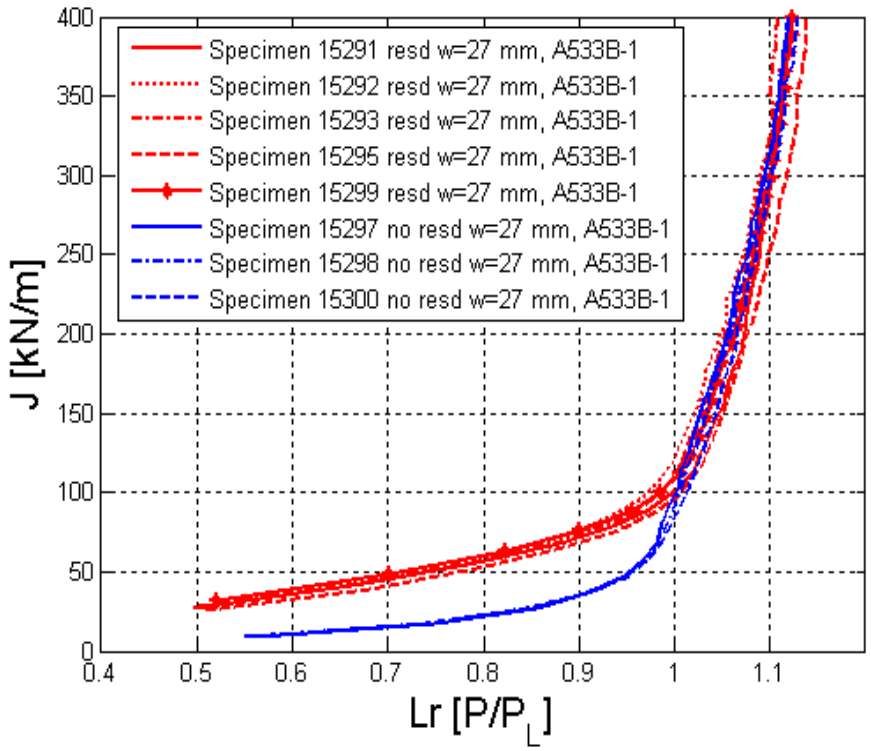

Figure 5.12: The *J*-integral results versus L_r for specimens with and without residual stresses.

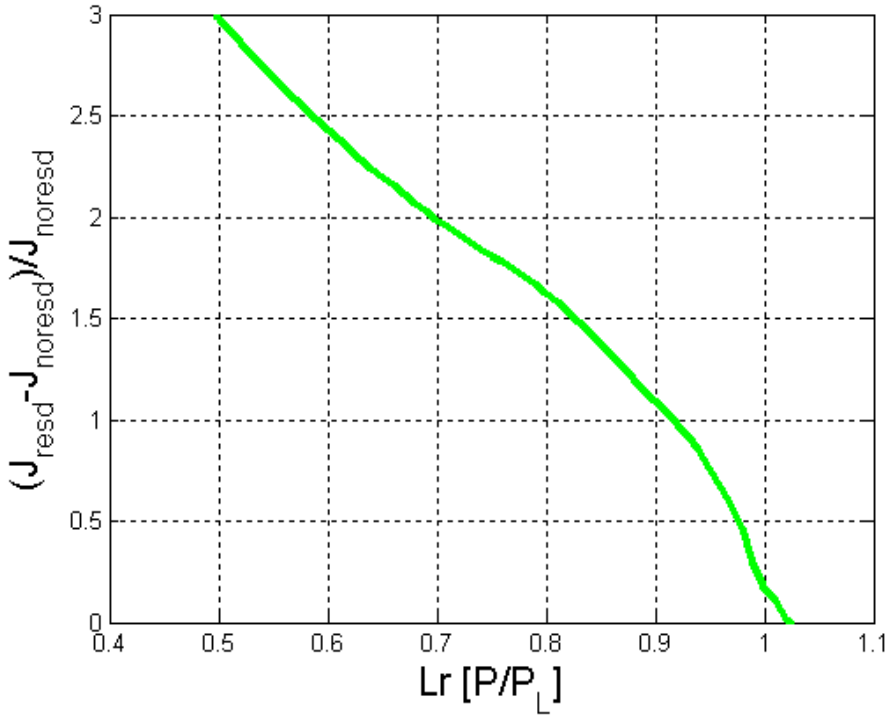

Figure 5.13: Relative difference in *J* between specimens with and without residual stresses.

From the colouring of these specimens during the tests it was concluded that the crack initiation occurred at L_r values between 1.05 and 1.1. No significant difference regarding crack initiation was observed between specimens with and without residual stresses.

Information on the crack growth, L_r and J-integral values in different specimens tested in test program 3 are presented in Table 5.3 for each colouring.

Table 5.3: Evaluated results for test program 3 at each colouring.

SPECIMEN	15291	15292	15293	15295	15299	15297	15298	15300
	PRE-LOADED	PRE-LOADED	PRE-LOADED	PRE-LOADED	PRE-LOADED	NO PRE-LOAD	NO PRE-LOAD	NO PRE-LOADED
				FIRST COLOURING				
ΔA [MM]	0.33	0.25	0.33	0.32	0.27	0.23	0.28	0.27
J [KN/M]	325	325	319	319	321	304	308	304
LR [PL/P]	1.11	1.10	1.10	1.12	1.11	1.10	1.11	1.10
				SECOND COLOURING				
ΔA [MM]	1.04	0.69	0.87	0.87	0.70	0.65	0.77	0.87
J [KN/M]	553	553	542	546	546	527	527	522
LR [PL/P]	1.10	1.14	1.13	1.15	1.15	1.13	1.13	1.13

It should be mentioned that two specimens were removed from the results presented above. The reason for the first removal was that the pre-loading was interrupted before reaching the final level, and the specimen was pre-loaded a second time. This could lead to unknown effects and therefore it was removed from the evaluated results. The second removed specimen showed higher stiffness than what was observed in all other specimens, as can be seen in Figure 5.14. The reason for this is still unclear, and therefore this specimen is also removed from the evaluated results.

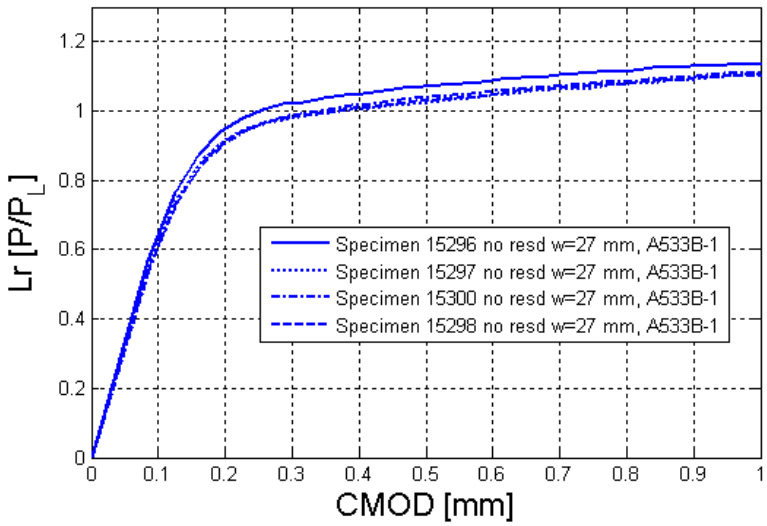

Figure 5.14: L_r-*CMOD* curve from test program 3 for all specimens without residual stresses.

6 ANALYSES BASED ON THE R6-METHOD

To investigate the inbuilt conservatism in the R6-method [19], the results obtained from the experimental programs are compared with results calculated using the R6 procedure. The experimental results are compared with both the R6 revision 3 option 1 curve (in ProSACC the R6 revision 3 option 1 curve is used) and with the approximate option 2 curve described in the R6-method, revision 4 [19].

6.1 Calculating *J* using R6

Calculating *J* using the R6-method uses the R6 function with the elastic solution of K_I to get an approximate elastic-plastic *J* solution. In the R6-method, the linear elastic stress intensity factor K_I is divided in two parts; one part from the secondary stresses K_I^S and one part from the primary stresses K_I^P. When secondary stresses are present, a ρ factor is also used in the calculations. More detailed description of the *J*-estimation approach is given in the R6-method revision-4 [19]. Below is a short description of how *J* is estimated in this study.

$$J(Lr) = \frac{\left(K_I^P + K_I^S\right)^2}{E'\left[f(Lr) - \rho\right]^2} \tag{6.1}$$

Where K_I^P is the linear elastic stress intensity factor derived from the primary load depending on L_r, K_I^S is the linear elastic stress intensity factor from the secondary stresses, $f(L_r)$ is the failure assessment curve in the R6-method, ρ is a correction factor depending on L_r, and E´ is the effective elastic modulus as defined below:

$$\begin{aligned} E' &= \frac{E}{1-\nu^2} \quad \text{for plane strain condition} \\ E' &= E \quad \text{for plane stress condition} \end{aligned} \tag{6.2}$$

Both the commonly used option 1 curve $f_1(L_r)$ found in R6 revision 3 and the approximate option 2 curve $f_2(L_r)$ from R6 revision 4 are used when estimating the *J* results. The option 1 curve $f_1(L_r)$ found in R6 revision 3 is independent of material behaviour while the approximate option 2 curve $f_2(L_r)$ from R6 revision 4 is material dependent. In Figure 6.1 the three different curves are shown.

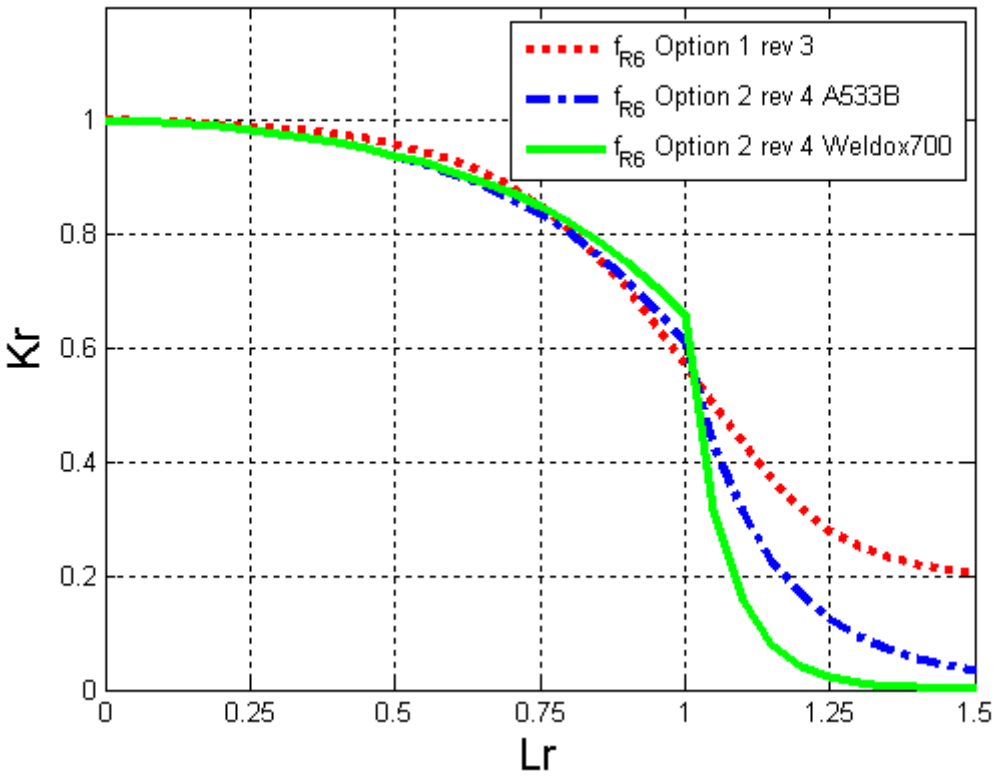

Figure 6.1: Different R6 curves used in the comparison with the experimental results.

Further the ρ factor is evaluated using the following expression,

$$\rho = \psi - \phi\left(\frac{K_I^S}{K_J^S} - 1\right), \tag{6.3}$$

where tabulated values of ψ and Φ are used [19]. A simplified procedure is also used for estimating of the ρ factor.

6.2 Comparison of estimated *J* with experimental results

In Figures 6.2 to 6.4 estimated J results using the R6-method with the option 1 curve are normalized with the results obtained from the experiments. The method used to approximate the J values presented below uses the same R6 curve and the same method of calculating the ρ factor as in ProSACC [1]. Values less than 1 indicates non conservative estimations of J while values above 1 indicates conservative results. As can be seen from the results in Figures 6.2 to 6.4, the estimations of J with residual stresses are significantly more conservative than those without residual stresses. Furthermore, it is seen in Figure 6.4 that the option 1 curve is non-conservative for L_r>1 for material A533B which has a Lüder strain region. It should be mentioned that according to the R6-method, Revision-4, for materials experiencing a Lüder strain region, the option 1 curve should not be used for L_r>1. It is also seen that the conservatism is rapidly decreasing for the Weldox 700 material for L_r>1, as shown in Figure 6.3 and 6.4. The explanation to this is the low hardening behaviour seen for Weldox 700 (R_{p02}/R_m=0.88). For a material with

low hardening the *J*-integral increases rapidly for high loads *Lr*>1. Since the option 1 curve is not material specific it does not consider the material hardening. Therefore the *J*-integral calculated by the R6 method using the option 1 curve, does not increase as rapidly for *Lr*>1 hence the drop in conservativeness seen in Figure 6.2 and 6.3. It should be noted that these results are seen to show the same trends as obtained by numerical analyses presented by James in a similar work conducted at SERCO [20].

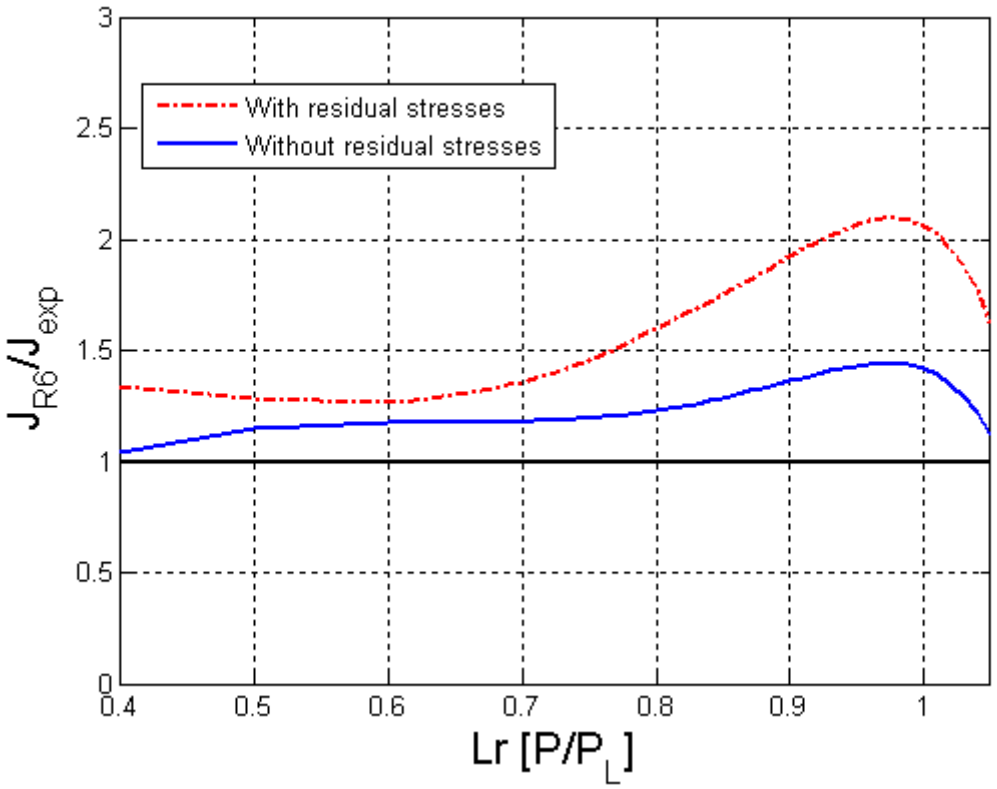

Figure 6.2: Estimated *J* results for test program 1 using the option 1 curve, normalized with experimentally evaluated *J* results, material Weldox 700.

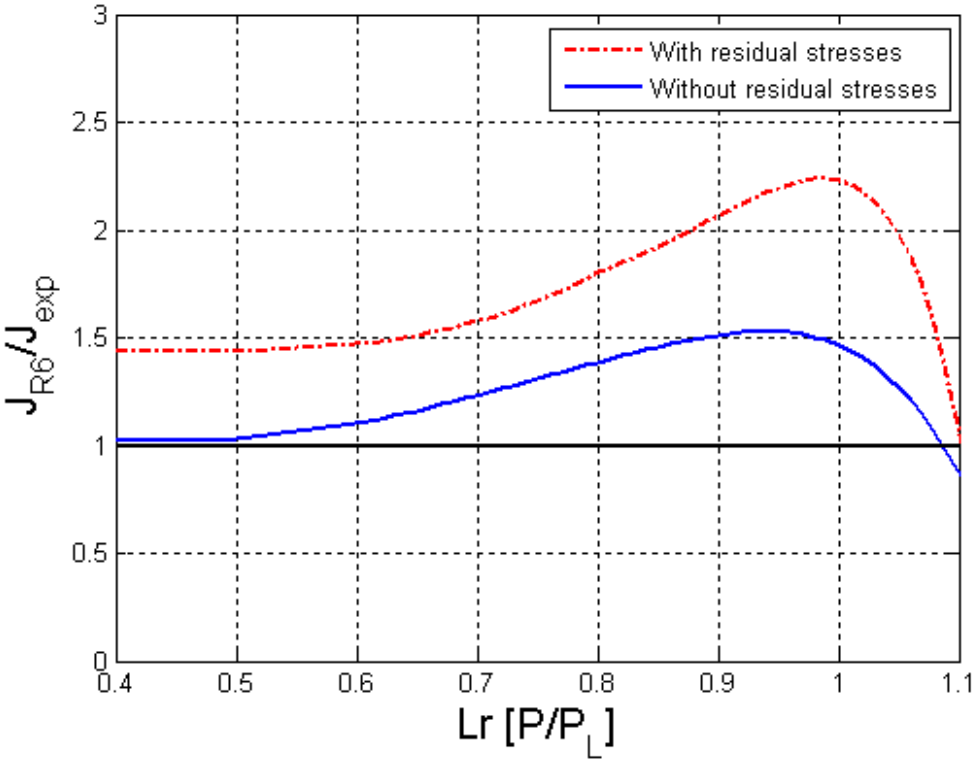

Figure 6.3: Estimated *J* results for test program 2 using the option 1 curve, normalized with experimentally evaluated *J* results, material Weldox 700.

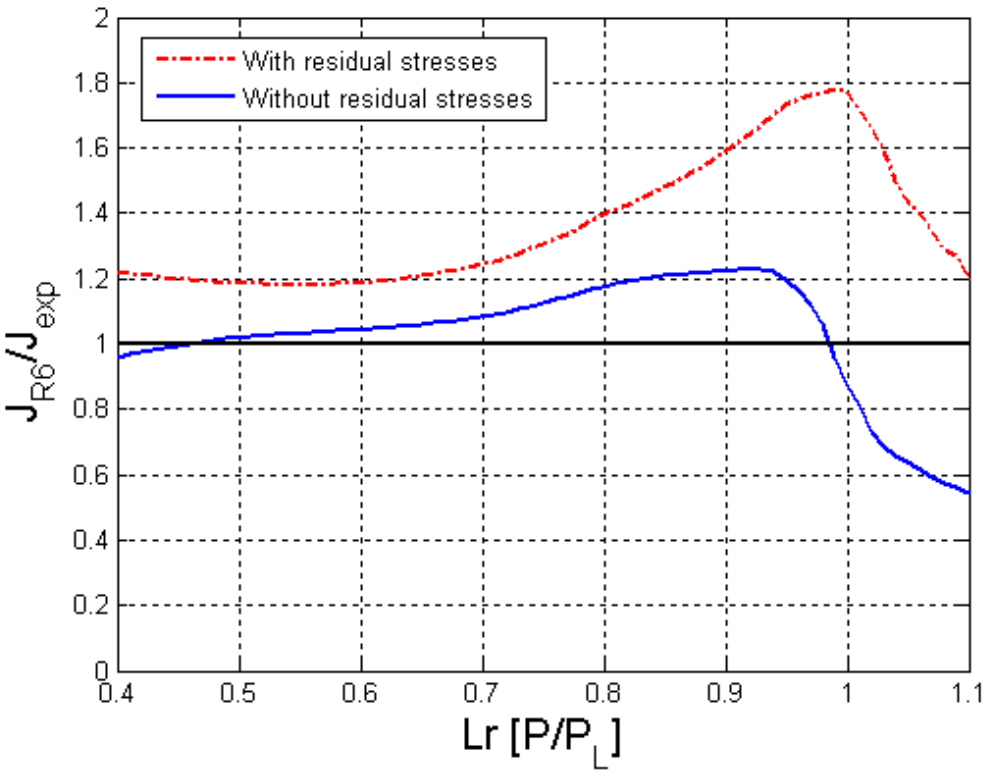

Figure 6.4: Estimated *J* results for test program 3 using the option 1 curve, normalized with experimentally evaluated *J* results, material A533B.

In Figure 6.5 to 6.7 the relative differences between the J results from specimens with and without residual stresses are plotted against L_r values. The green curves are J values obtained from the experiments, the red curves are obtained using the R6-method to calculate J while the blue curves are obtained using the proposed new analyse strategy in [8] to calculate J. The new analyse strategy is discussed more in chapter 7. As can be observed, the relative differences for J obtained from the experiments drop much more rapidly than the relative differences for J obtained using the R6-method. The aim with the proposed new analyse strategy in [8] is to lessen the gap seen between the experimental results and the R6 results at high load levels. With the new analysis strategy the calculated J values are seen to be closer to the experimental results. This is in good agreement with the observations from the numerical analyses presented by Dillström et al in proposing a new assessment strategy [8]. The results from the R6 assessments where obtained using the option 1 curve and ρ factor.

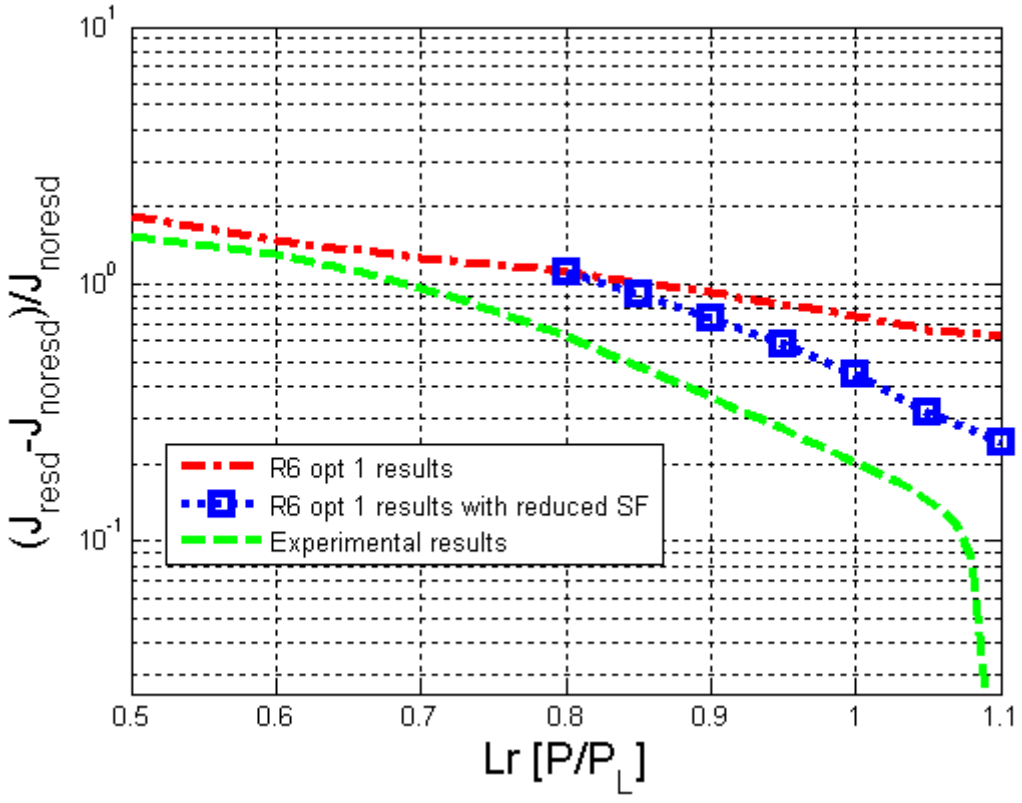

Figure 6.5: Relative difference in J between specimens with and without residual stresses from test program 1 (Weldox700, W=100mm).

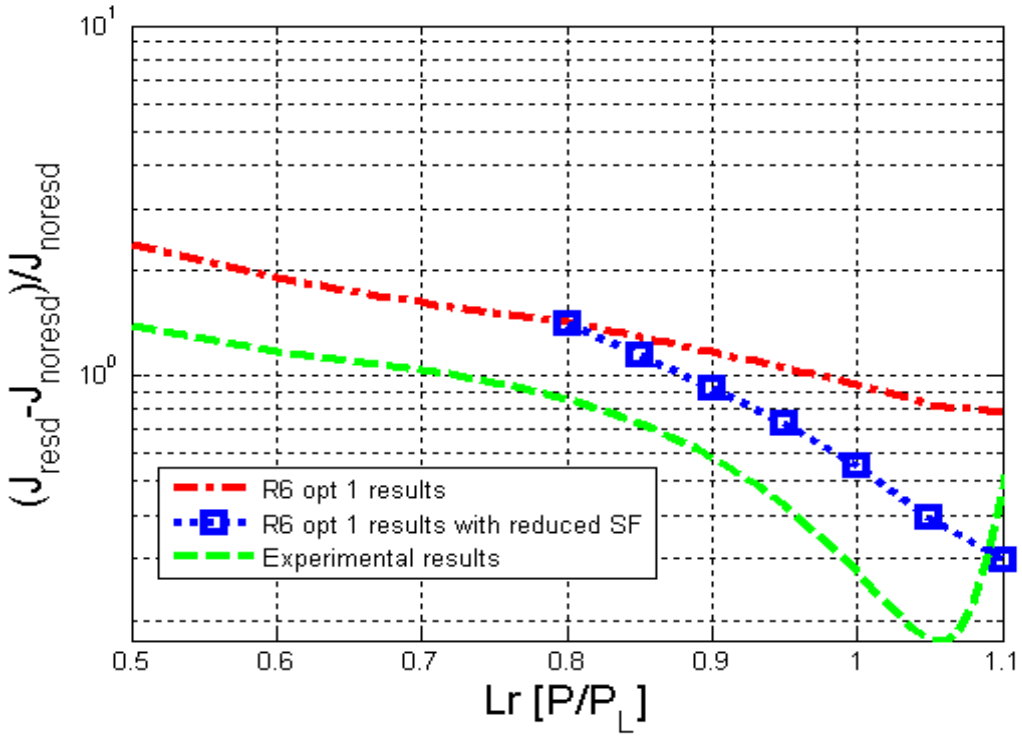

Figure 6.6: Relative difference in *J* between specimens with and without residual stresses from test program 2 (Weldox700, W=70mm).

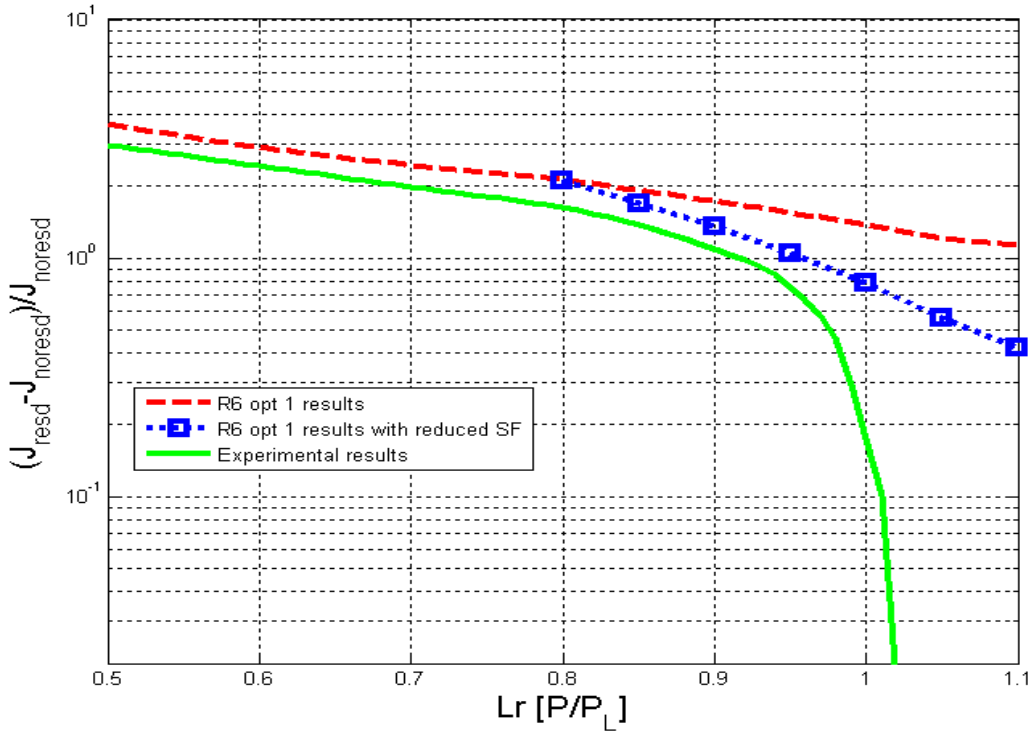

Figure 6.7: Relative difference in *J* between specimens with and without residual stresses from test program 3 (A533B, W=27mm).

In Figures 6.8 to 6.10 the normalized *J* results evaluated using the option 2 curve are presented. The results are normalized by the *J* values obtained from the experiments. Similar to the results

using the option 1 curve, it is observed here that the estimations of J with residual stresses are significantly more conservative than those without residual stresses. But for the option 2 curves, the level of conservatism does not decrease for L_r>1. A drop in conservatism is seen at L_r=1, but for L_r>1 the conservatism rapidly increases again. It should be noted that these results are seen to show the same trends as obtained by numerical analyses presented by James [20].

From all the presented results in Figures 6.2 to 6.10, it is observed that the inbuilt over-conservatism in the R6 procedure is very clear when residual stresses are present both for the option 1 curve and the option 2 curve for L_r<1. The increase starts around L_r=0.7 in all cases and continue increasing until L_r≈0.9-1.0 where it starts to drop for some cases. For the option 1 curves the drop continue for L_r>1 but for the option 2 curves the conservatism starts to rapidly increase for L_r>1. It should be noted that the drop in the conservatism of the R6-method observed for some cases in Figures 6.8 and 6.9 for L_r<1, is rather small and do not lead to any non-conservatism for the cases with residual stresses.

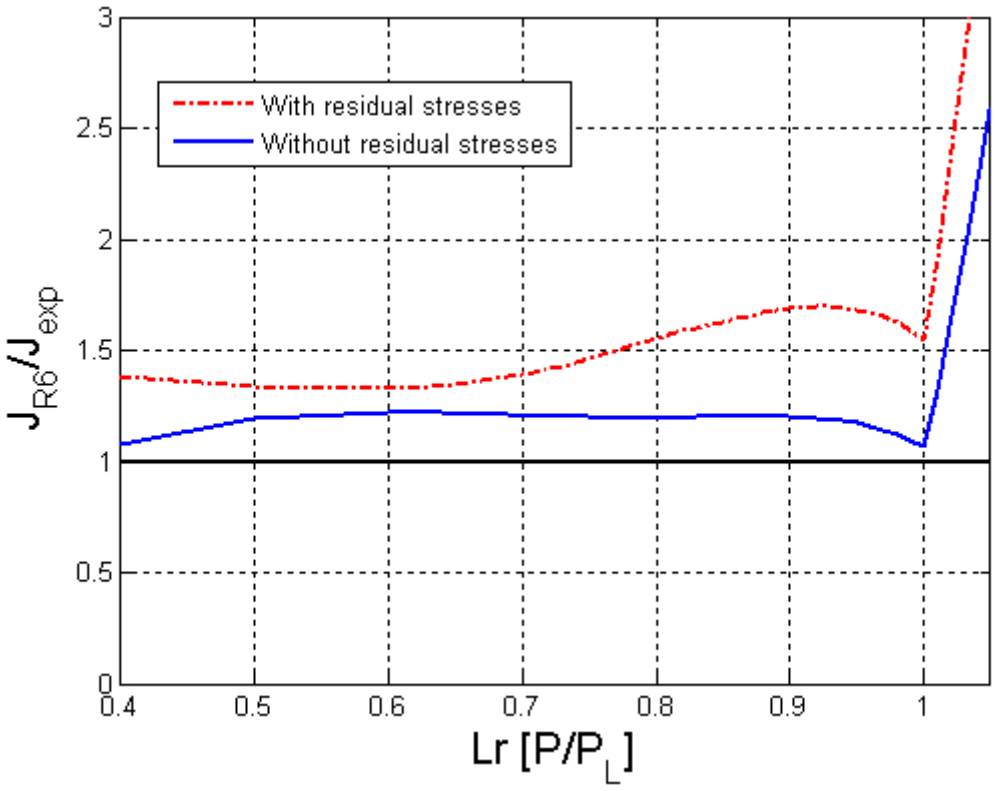

Figure 6.8: Estimated J results for test program 1 using the option 2 curve, normalized with experimentally evaluated J results, material Weldox 700.

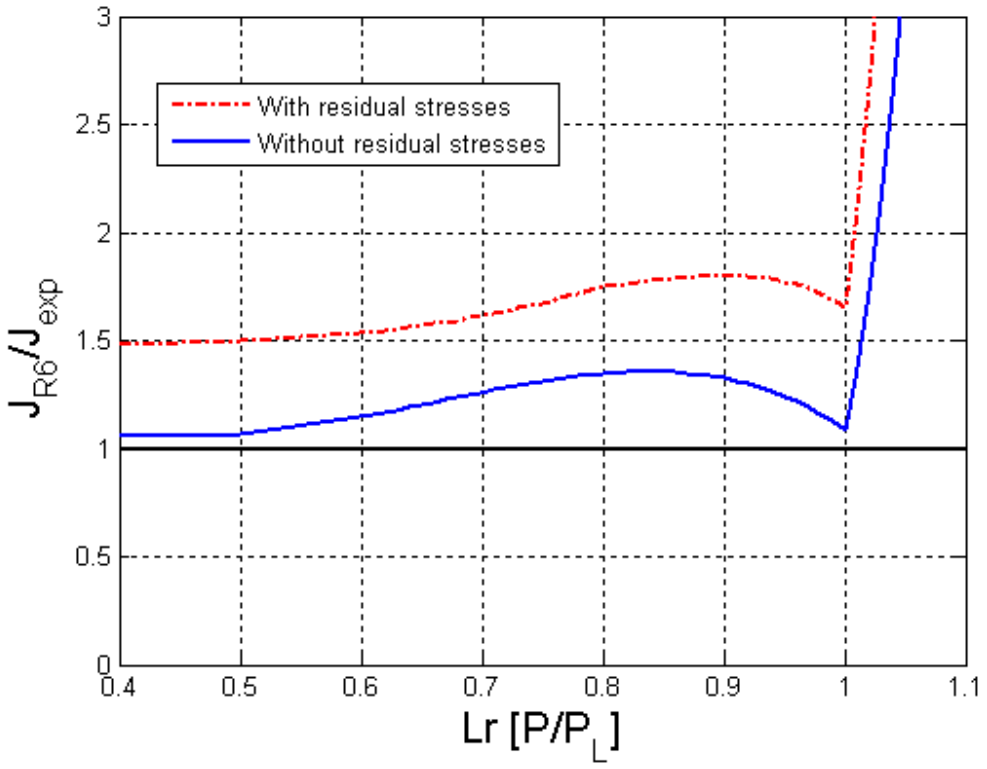

Figure 6.9: Estimated *J* results for test program 2 using the option 2 curve, normalized with experimentally evaluated *J* results, material Weldox 700.

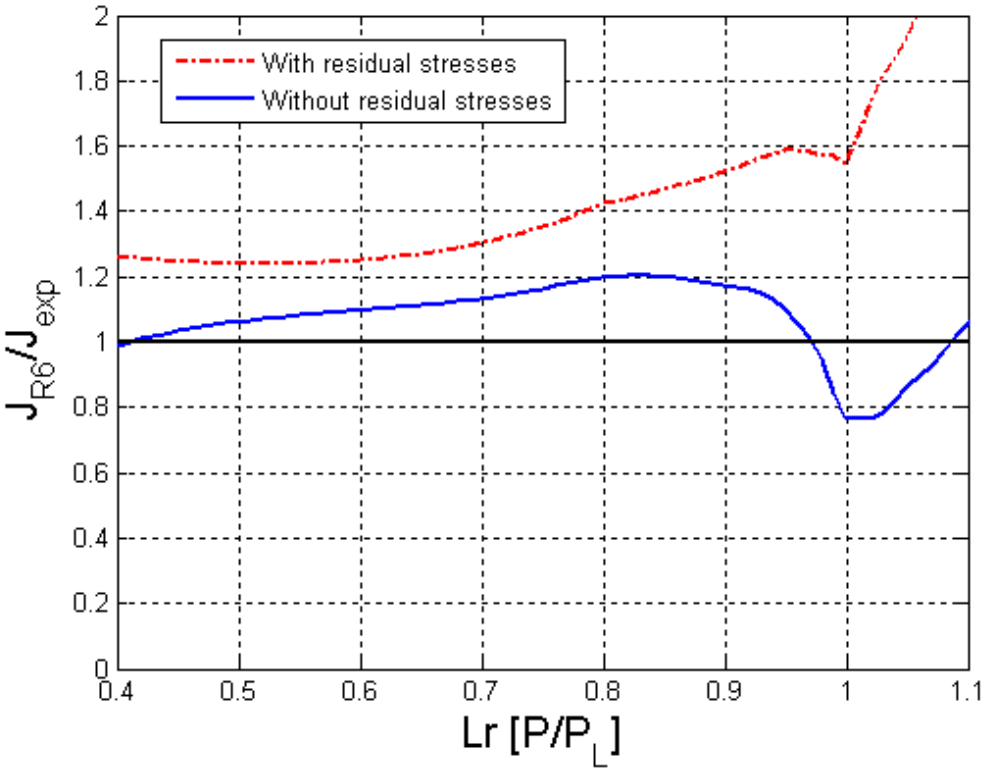

Figure 6.10: Estimated *J* results for test program 3 using the option 2 curve, normalized with experimentally evaluated *J* results, material A533B.

7 VERIFICATION OF THE PROPOSED ANALYSIS STRATEGY

The significance of the secondary stresses for defects (cracks) in ductile materials within nuclear applications was previously studied by Dillström et al [8] by conducting numerical analysis on cracked bodies. Both thin-walled and thick-walled pipes containing surface cracks were studied, where the relative contribution from the weld residual stresses to the *J*-integral was calculated. These results showed that the relative contribution to *J* dropped at a much higher rate for high *Lr* values in the numerical studies compared with results obtained from ProSACC. This leads to overly conservative results for high *Lr* values when using ProSACC. This is also seen in the results from the current experimental study see Figure 6.5, 6.6 and 6.7.

Based on the outcome of the study in [8], an analysis strategy for fracture assessment of defects in ductile materials of nuclear components has been proposed to more realistically handle the contribution of secondary stresses to the fracture parameters *J*. According to this new Analysis Strategy, new safety factors are defined that differentiate between primary stresses and secondary stresses. The new safety factors against fracture described by K_I and differentiate between $SF_K^{primary}$ (relating to primary stresses) and $SF_K^{secondary}$ (relating to secondary stresses). The purpose with this new strategy is to reduce the conservatism in handling of secondary stresses in ProSACC i.e. lessen the gap between the curves in Figure 6.5, 6.6 and 6.7.

According to the new Analysis Strategy, the safety factors related to secondary stresses decrease based on the predicted value of *Lr* at fracture. The idea is shown in Figure 1.1, indicating that the contribution from secondary stresses becomes negligible for high L_r-values. The predicted value of *Lr* at fracture is calculated by first doing a standard handbook analysis to get an evaluation point within the R6-diagram. Secondly the primary load is increased until the R6 curve intersects. This *Lr* value at the intersection point should be used in determining the new safety factor $SF_K^{secondary}$. It is suggested that the weight down on $SF_K^{secondary}$ starts at L_r= 0.8, going down to unity at L_r = 1.2 for ductile materials.

The obtained results in this study, presented in Chapters 5 and 6, that are obtained from experimental and numerical analyses on different materials and cracked specimens do verify the Analysis Strategy proposed in [8].

The relative differences in the *J*-integral in different specimens with and without residual stresses tested in test programs 1 to 3 are presented in Chapter 6, and are shown again in Figure 7.1. These results do strengthen the deterministic safety evaluation system suggestion in [8] to divide the safety factor in two separate safety factors; one as $SF_K^{primary}$ for primary stresses and one as $SF_K^{secondary}$ for secondary stresses. $SF_K^{secondary}$ can be weighted down depending on the predicted value of Lr at fracture. In the new Analysis Strategy [8], it is suggested to start the weighting down of the secondary safety factor $SF_K^{secondary}$ for a predicted fracture at *Lr*=0.8. The results presented in Figure 7.1 clearly show that this is reasonable. Further in [8], it is also suggested that the secondary safety factor $SF_K^{secondary}$ can even be lowered towards zero for *Lr*> 1. The presented results can not strictly verify this but there is a clear trend seen for the results that the influence from the residual stresses start to diminish for *Lr*>1.

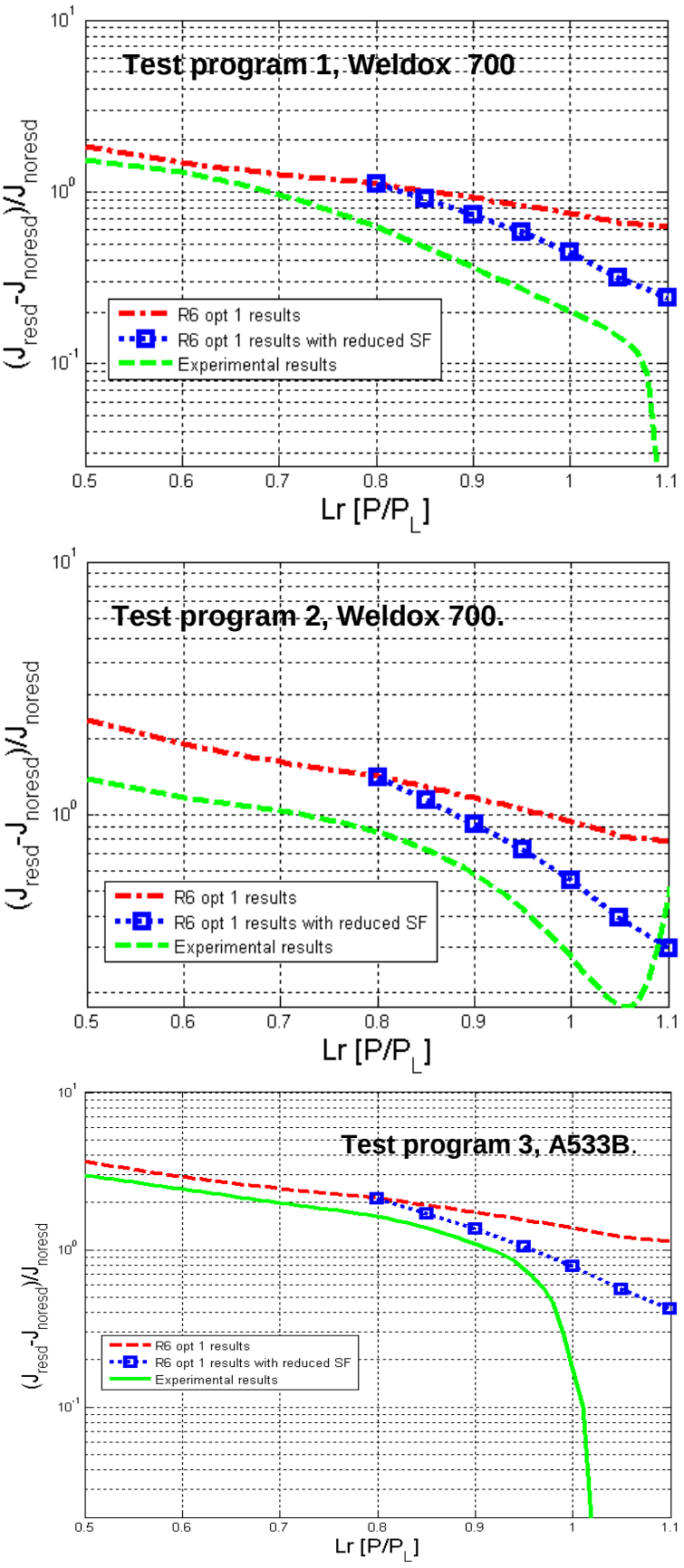

Figure 7.1: The relative differences in the *J*-integral in different specimens with and without residual stresses tested in test programs 1 to 3.

8 CONCLUSIONS

Based on the experimental and numerical investigation on the effects of residual stresses in cracked specimens of ductile materials the following conclusions may be made:

- The experimental results clearly show a decreasing influence from the residual stresses on the *J*-integral for increasing primary load. A clear trend could be seen for both material that the influence from the residual stresses start to disappear entirely for $Lr>1$. For the material A533B the influence from the residual stresses on *J* was seen to disappear entirely for $Lr>1$.
- Crack initiation in the experiments was achieved at L_r values between 0.9-1.1. Only small effects from the residual stress field were seen on crack initiation for the specimens which had crack initiation at L_r values between 0.9 and 1.0, and no effects from the residual stress field on crack initiation were seen for the specimens loaded at L_r values between 1.0 and 1.1.
- It was shown that the residual stress field had no measurable influence on the stable crack growth of the specimens at $L_r> 1$.
- The experimental results did not show any apparent effect from the received residual stress field on the material fracture toughness of the used materials, Weldox 700 and A533B.
- The estimated *J* results with the R6 procedure using the option 1 curve revision 3 shows high inbuilt conservativeness for specimens with residual stresses at $Lr<1.0$. The conservativeness starts to increase at $Lr>0.7$ up to $Lr=1.0$ where it starts to drop.
- The different options for the R6 curve show different levels of conservativeness. The option 1 curve in revision 3 (used in ProSACC) show a higher level of conservativeness for specimens with residual stresses at $L_r< 1$, but for $L_r> 1$ the option 2 curve in revision 4 shows higher conservativeness for specimens with and without residual stresses.
- The presented results strengthen the validity of the suggested deterministic safety evaluation system proposed by Dillström et al [8], where it is suggested to start the weighting down of the secondary safety factor $SF_K^{secondary}$ at a predicted value at fracture of $L_r=0.8$. The suggested evaluation system is valid for sufficiently ductile materials such as austenitic stainless steels, nickel based alloys and ferritic steels in the upper shelf regime.

9 REFERENCES

[1] DILLSTRÖM, P., ANDERSSON, P., BERGMAN, M., BRICKSTAD, B., DAHLBERG, L., NILSSON, F., SATTARI-FAR, I., SUND, G. AND ZANG, W., (2008), "A COMBINED DETERMINISTIC AND PROBABILISTIC PROCEDURE FOR SAFETY ASSESSMENT OF COMPONENTS WITH CRACKS-HANDBOOK", REPORT NUMBER 2008:01, STRÅLSÅKERHETSMYNDIGHETEN (SSM).

[2] SHARPLES, J. K., HARRISON, M., MAY, K. A., CHIVERS, T. C. AND SMITH, E., (1993), "THE EFFECT OF RESIDUAL STRESSES ON FRACTURE BEHAVIOUR", PRESSURE VESSEL INTEGRITY, ASME-PVP, VOL. 250, PP. 105-113.

[3] SHARPLES, J. K., SANDERSON, D. J., BOWDLER, B. R., WIGHTMAN, A. P. AND AINSWORTH, R. A., (1995) "EXPERIMENTAL PROGRAMME TO ASSESS THE EFFECT OF RESIDUAL STRESSES ON FRACTURE BEHAVIOUR", ASME-PVP, VOL. 304, PP. 539-551.

[4] SHARPLES, J. K. AND GARDNER, L., (1996), "DUCTILE TEARING TESTS OF 316 STAINLESS STEEL WIDE PLATES CONTAINING WELDMENTS", INT. JOUR OF PRES. VES. & PIPING, VOL. 65, PP. 353-363.

[5] MIRZAEE_SISAN, A., TRUMAN, C. E., SMITH, D.J. AND SMITH, M.C. (2007) "INTERACTION OF RESIDUAL STRESS WITH MECHANICAL LOADING IN A FERRITIC STEEL", ENG. FRACT. MECH. VOL. 74, PP. 2864-2880.

[6] MIRZAEE_SISAN, A., TRUMAN, C. E., SMITH, D.J. AND SMITH, M.C. (2007) "INTERACTION OF RESIDUAL STRESS WITH MECHANICAL LOADING IN AN AUSTENITIC STAINLESS STEEL", FATIGUE. FRACT. ENGNG. MATER. STRUCT. VOL. 31, PP. 223-233.

[7] SATTARI-FAR, I., (2008) "PRELIMINARY STUDY ON CONDUCTING EXPERIMENTS FOR ASSESSMENT OF SECONDARY STRESSES", INSPECTA/FOU-REPORT NO.: 2008/02, INSPECTA TECHNOLOGY AB, SWEDEN.

[8] DILLSTRÖM, P., ANDERSSON, M., SATTARI-FAR, I. AND ZHANG, W., (2009), "ANALYSIS STRATEGY FOR FRACTURE ASSESSMENT OF DEFECTS IN DUCTILE MATERIAL", REPORT NUMBER 2009:27, STRÅLSÅKERHETSMYNDIGHETEN (SSM).

[9] HIBBIT, KARLSSON AND SORENSON, (2009), ABAQUS USER MANUAL, V. 6.9, DASSAULT SYSTÈMES.

[10] ASTM STANDARD TEST METHOD OF MEASUREMENT OF FRACTURE TOUGHNESS, E 1820.

[11] LEMAITRE, J. AND CHABOCHE, J.-L., (1990), "MECHANICS OF SOLID MATERIALS", CAMBRIDGE UNIVERSITY PRESS.

[12] CORRESPONDENCE WITH ABAQUS'S USER SUPPORT, 2010.

[13] ZHU, X. K., LEIS, B. N. AND JOYCE, A., (2008), "EXPERIMENTAL ESTIMATION OF J-R CURVES FROM LOAD-CMOD RECORD FOR SE(B) SPECIMENS", J. ASTM INT., VOL. 5, NO. 5, PAPER ID JAI101532.

[14] SAADATI, M., (2010), "J-INTEGRAL EVALUATION IN 2D AND 3D CRACK PROBLEMS WITH RESIDUAL STRESS FIELDS" INSPECTA RESEARCH REPORT NO. 50010720, REV 0.

[15] LEI, Y., O ´DOWD, N. P. AND WEBSTER, G. A., (2000), "FRACTURE MECHANICS ANALYSIS OF A CRACK IN A RESIDUAL STRESS FIELD", INT. J. FRACTURE, VOL 106, PP. 195-216.

[16] LEI, Y., (2005), "J-INTEGRAL EVALUATION FOR CASES INVOLVING NON-PRPOTIONAL STRESSING", ENGINEERING FRACTURE MECHANICS, VOL. 72, PP. 577-596.

[17] VON UNGE, P., (2008), "CALCULATION METHODS FOR CRACKS IN RESIDUAL STRESS FIELDS", INSPECTA RESEARCH REPORT NO. 50008280, REV 0.

[18] DILLSTRÖM, P. AND SATTARI-FAR, I., (2003), "LIMIT LOAD SOLUTIONS FOR SURFACE CRACKS IN PLATES AND CYLINDERS", DNV RSE R&D REPORT NO. 2002/01, REV. 2, DET NORSKE VERITAS, SWEDEN.

[19] R6 REVISION 4, AMENDMENT NR. 8, (2010) "ASSESSMENT OF THE INTEGRITY OF STRUCTURES CONTAINING DEFECTS", BRITISH ENERGY GENERATION LTD.

[20] JAMES, P. M., (2008), "CONTINUING DEVELOPMENT OF A SIMPLIFIED METHOD TO ACCOUNT FRO THE INTERACTION OF PRIMARY AND SECONDARY STRESSES", PROCEEDINGS OF ASME PVP 2008, PVP2008-61040.

2011:19

The Swedish Radiation Safety Authority has a comprehensive responsibility to ensure that society is safe from the effects of radiation. The Authority works to achieve radiation safety in a number of areas: nuclear power, medical care as well as commercial products and services. The Authority also works to achieve protection from natural radiation and to increase the level of radiation safety internationally.

The Swedish Radiation Safety Authority works proactively and preventively to protect people and the environment from the harmful effects of radiation, now and in the future. The Authority issues regulations and supervises compliance, while also supporting research, providing training and information, and issuing advice. Often, activities involving radiation require licences issued by the Authority. The Swedish Radiation Safety Authority maintains emergency preparedness around the clock with the aim of limiting the aftermath of radiation accidents and the unintentional spreading of radioactive substances. The Authority participates in international co-operation in order to promote radiation safety and finances projects aiming to raise the level of radiation safety in certain Eastern European countries.

The Authority reports to the Ministry of the Environment and has around 270 employees with competencies in the fields of engineering, natural and behavioural sciences, law, economics and communications. We have received quality, environmental and working environment certification.

Strålsäkerhetsmyndigheten
Swedish Radiation Safety Authority

SE-171 16 Stockholm
Solna strandväg 96

Tel: +46 8 799 40 00
Fax: +46 8 799 40 10

E-mail: registrator@ssm.se
Web: stralsakerhetsmyndigheten.se